

A statistical study of the spatial distribution of Co-operative UK Twin Located Auroral Sounding System (CUTLASS) backscatter power during EISCAT heater beam-sweeping experiments

H. Shergill,¹ T. R. Robinson,¹ R. S. Dhillon,¹ M. Lester,¹ S. E. Milan,¹ and T. K. Yeoman¹

Received 17 July 2009; revised 26 September 2009; accepted 20 November 2009; published 14 May 2010.

[1] High-power electromagnetic waves can excite a variety of plasma instabilities in Earth's ionosphere. These lead to the growth of plasma waves and plasma density irregularities within the heated volume, including patches of small-scale field-aligned electron density irregularities. This paper reports a statistical study of intensity distributions in patches of these irregularities excited by the European Incoherent Scatter (EISCAT) heater during beam-sweeping experiments. The irregularities were detected by the Co-operative UK Twin Located Auroral Sounding System (CUTLASS) coherent scatter radar located in Finland. During these experiments the heater beam direction is steadily changed from northward to southward pointing. Comparisons are made between statistical parameters of CUTLASS backscatter power distributions and modeled heater beam power distributions provided by the EZNEC version 4 software. In general, good agreement between the statistical parameters and the modeled beam is observed, clearly indicating the direct causal connection between the heater beam and the irregularities, despite the sometimes seemingly unpredictable nature of unaveraged results. The results also give compelling evidence in support of the upper hybrid theory of irregularity excitation.

Citation: Shergill, H., T. R. Robinson, R. S. Dhillon, M. Lester, S. E. Milan, and T. K. Yeoman (2010), A statistical study of the spatial distribution of Co-operative UK Twin Located Auroral Sounding System (CUTLASS) backscatter power during EISCAT heater beam-sweeping experiments, *J. Geophys. Res.*, 115, A05307, doi:10.1029/2009JA014659.

1. Introduction

[2] The generation of field-aligned irregularities (FAIs) in the ionospheric plasma density was one of the most unexpected results of early ionospheric modification experiments carried out at the midlatitude heating facility in Platteville, Colorado (40.2°N, 104.7°W). Intentional modification of the ionosphere began there in 1970 in order to study the interaction of ionospheric plasma waves with high-power radio waves transmitted by a “heater” or “pump”. Observations made between 1970 and 1973 revealed a number of characteristics of the FAIs [e.g., *Thome and Blood*, 1974; *Fialer*, 1974; *Minkoff et al.*, 1974] involving their growth and decay times, preconditioning effects, and the dependence of the scattered signal strength on radar orientation.

[3] Experiments carried out with the Platteville heater prompted the building of similar facilities in the United States, the former Soviet Union, and northern Scandinavia [*Yampolski et al.*, 1997; *Hughes et al.*, 2003; *Noble and Djuth*, 1990]. Between 1977 and 1980 a high-latitude heating facility was built near Tromsø, Norway (69.6°N,

19.2°E). Observations made at this heater have confirmed the ubiquity and importance of FAI in heating experiments [e.g., *Stubbe et al.*, 1982a]. In particular, it is thought that FAIs lead to anomalous absorption of the high-power pump [e.g., *Jones et al.*, 1982; *Stubbe et al.*, 1982a; *Robinson*, 1989], which in turn leads to large-scale heating [e.g., *Jones et al.*, 1986; *Stocker et al.*, 1992; *Honary et al.*, 1993].

[4] Direct measurements of FAI at Tromsø have been made using the Co-operative UK Twin Located Auroral Sounding System (CUTLASS) coherent backscatter radars in Finland and Iceland since these radars became operational in 1995 [*Robinson et al.*, 1997, 1998]. In one early experiment using the CUTLASS radar, *Bond et al.* [1997] studied the form of the CUTLASS backscatter power distribution in patches of irregularities enhanced by the European Incoherent Scatter (EISCAT) heater, both in range and in azimuth, using static beam configurations. The distributions were found to be approximately Gaussian, and the widths of the patches extended beyond that of the heater beam at its 3 dB points. However, it remains unclear what mechanisms control the distribution of the irregularities created by the heater at Tromsø. A number of different contributing factors have been suggested. These clearly include the power distribution in the heater beam itself and the influence of the magnetic field, which can affect both the refraction of heater rays and the anisotropic transport of electrons. In addition,

¹Department of Physics and Astronomy, University of Leicester, Leicester, United Kingdom.

there is much evidence that mode conversion of radio waves into electrostatic modes at the upper hybrid resonance is responsible for the generation of FAIs [Stubbe *et al.*, 1982b; Robinson, 1989, 2002]. Access to this resonance region by heater rays can thus influence where FAI can be excited. An experiment designed to explore further the distribution of irregularities is outlined below. This experiment has enabled some of these dependences to be tested. This uses a beam-sweeping technique to extend the area of the illumination of the ionosphere beyond the static beam geometry. The measured CUTLASS backscatter intensity distributions from irregularity patches are analyzed using a statistical method that yields information about the location and shape of the patches. This involves a moment analysis of the spatial distribution of the intensity of CUTLASS backscatter. This method of analysis is ideal for investigating spatial distributions as it allows them to be characterized by just a few parameters without the need to examine a large number of individual data points. Using this method, we compare the beam shape and irregularity distribution shape for a number of experimental configurations. In addition, a simple geometrical model based on the upper hybrid theory of FAI excitation is examined by this method. Before dealing with the experimental data, and to provide a basic geometrical framework for describing and interpreting the results, a simple upper hybrid FAI generation model is outlined in the next section.

2. A Simple Upper Hybrid Model

[5] In a horizontally stratified ionosphere an O -mode radio ray transmitted at an angle from vertical that is less than the Spitze angle, θ_S [Mjølhus and FLÅ, 1984; Mjølhus *et al.*, 2003], reflects at an altitude where the local electron plasma frequency is equal to the frequency of the transmitted wave, ω . The O -mode radio waves transmitted at an angle θ from vertical that is greater than the Spitze angle reflect at a lower altitude than this. As long as the radio propagation frequency is at least a few times the electron gyrofrequency, ω_H , then the reflection occurs approximately at an altitude where [Davies, 1966]

$$\omega = \omega_p \sec \theta \quad (1)$$

such that greater off-zenith transmission angles cause the electromagnetic wave to reflect at lower altitudes. This is termed the secant law.

[6] In the upper hybrid plane, U , resonant conversion of an O -mode radio wave into upper hybrid wave modes can lead to the enhancement of electron density irregularities in the ionospheric plasma and additional anomalous plasma heating. This plane occurs where the heater frequency equals the upper hybrid resonance frequency, ω_U , which obeys the relationship [e.g., Das and Fejer, 1979; Robinson, 1989]

$$\omega_U^2 = \omega_p^2 + \omega_H^2. \quad (2)$$

Thus, the upper hybrid plane lies at an altitude h_U above the ground, between the reflection planes of the vertically transmitted O - and X -mode waves. Therefore, only O -mode radio waves transmitted by the heater should be able to

enhance FAIs, and this has been observed experimentally [e.g., Cohen and Whitehead, 1970; Jones *et al.*, 1982; Robinson *et al.*, 1998].

[7] The secant law, equation (1), and upper hybrid relation, equation (2), can be combined to produce a simple model that provides a horizontal width limit and position for the patches of FAIs enhanced by the heater in the upper hybrid plane. Considering equation (1) with the requirement for radio waves to reach an altitude h_U for FAI enhancement to occur implies that if the heater beam transmission angle is great enough, then U is not reached by the transmitted waves, and plasma density irregularities should not be enhanced there. This situation is illustrated schematically in Figure 1, which shows a simplified estimate of where the patches of irregularities may be positioned, assuming rectilinear propagation of the heater waves, with no refraction. The reflection plane of a vertically transmitted O -mode wave and the upper hybrid plane, U , are shown as dotted and dashed lines, respectively. The critical transmission angle, θ_C , and the limiting upper hybrid width of the patch of irregularities, w_U , are given by

$$\theta_C = \sin^{-1} \left(\frac{\omega_H}{\omega} \right) \quad (3)$$

and

$$w_U = 2h_U \tan \theta_C, \quad (4)$$

respectively. The reflection condition for heater rays transmitted at different angles from vertical, equation (1), places a restriction on the area within which the rays are able to reach U , and the irregularities are expected to change form, depending on where the heater beam is directed. This is particularly the case if the heater beam is pointed outside of the critical angle given by equation (3). It should be noted that, given horizontal stratification, the conditions set by equations (3) and (4) represent a potential access window for excitation of irregularities at h_U that is not affected by any changes in the beam pointing direction. However, if stratification of the ionosphere were tilted, then the positions of the width limits would be shifted horizontally. A 10° tilt in the ionospheric stratification results in an approximate 30 km horizontal shift and 5 km change in width. Ionospheric tilts therefore might cause a shift in the position of patches of FAIs from that expected from Figure 1.

3. Instrumentation

[8] This study mainly utilizes coherent backscatter data from the CUTLASS backscatter radar in Finland [Milan *et al.*, 1997] to provide information about the spatial distribution of FAI produced by the Tromsø heater. However, data from the EISCAT UHF radar [Rishbeth and Williams, 1985] and the Tromsø dynasonde [Sedgemore *et al.*, 1996; Jones *et al.*, 2000] have also been used to provide information about the background ionosphere. These systems and the EISCAT heater are briefly described below.

3.1. European Incoherent Scatter (EISCAT) Heater

[9] The ionospheric modification facility situated at Ramfjordmoen near Tromsø, Norway, was built by the Max-Planck-Institut für Aeronomie and the University of

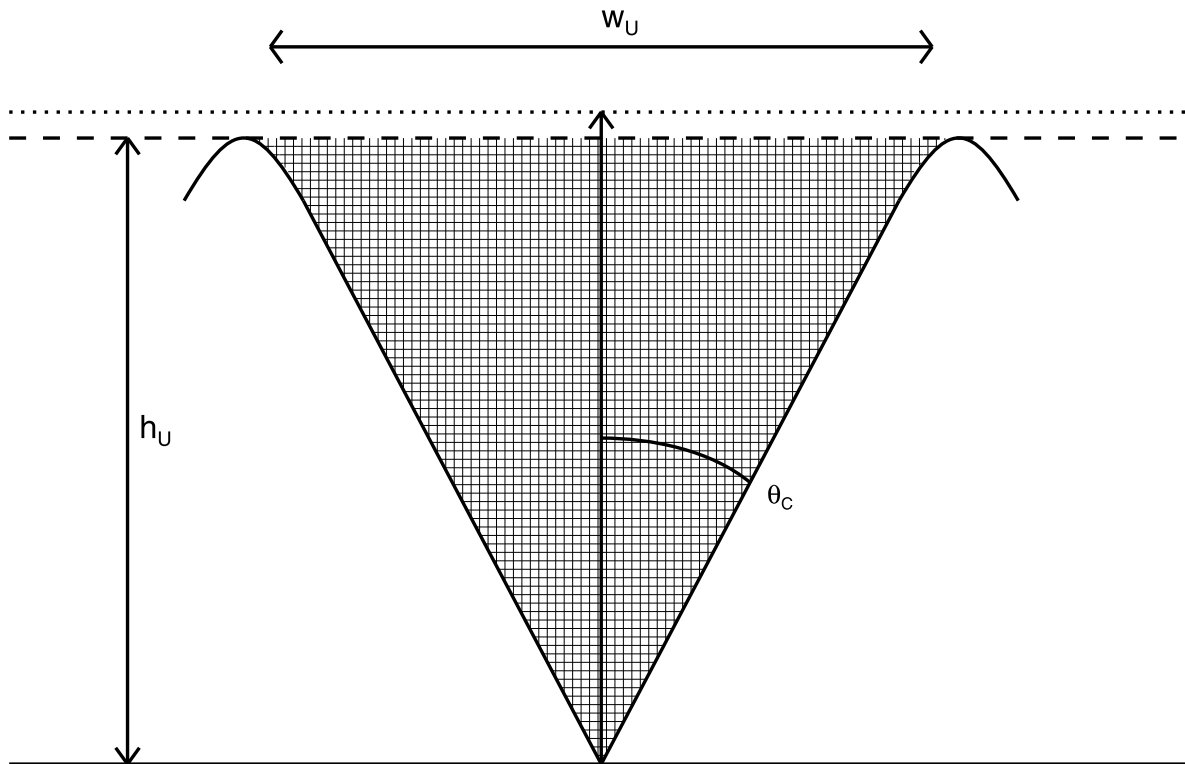


Figure 1. A simple representation of transmitted radio waves and their planes of reflection. The dotted line indicates the plane of reflection of a vertically transmitted radio wave, and the dashed line indicates the upper hybrid plane, the plane of reflection of a radio wave transmitted at an angle θ_C from vertical. Rays transmitted at angles within the shaded region will reflect at or above the upper hybrid height. Rays transmitted at angles outside of the shaded region will not reach the upper hybrid height.

Tromsø, although it is now operated by the EISCAT Scientific Association [Rietveld *et al.*, 1993]. The heating facility has 12 transmitters, with output powers of up to 100 kW each, and has three antenna arrays of different frequency ranges. Array 2, which was used during the beam-sweeping experiments studied here, contains six rows of six crossed dipoles, covers the frequency range 3.75–5.65 MHz, and has a gain of 24 ± 1 dB. This produces a beam width of 14.5° and a maximum effective radiated power (ERP) of 300 MW. The beam width increases if fewer than the maximum number of transmitters is used, due to the widening of the interference pattern that is produced.

[10] The frequency, polarization, beam direction, and maximum power of the heater are normally set up during tuning; however, these parameters can be changed during a heating experiment without the need to retune. The east-west orientation of the dipole antennas allows the heater beam pointing direction to be tilted in the north-south plane by varying the phases between pairs of transmitters driving each row of antennas.

3.2. Co-operative UK Twin Located Auroral Sounding System (CUTLASS)

[11] CUTLASS forms part of the Super Dual Auroral Radar Network (SuperDARN) of high-frequency backscatter radars [Greenwald *et al.*, 1995]. The radars use coherent backscatter to study Earth's upper atmosphere and ionosphere. The field-aligned nature of the irregularities requires

the wave vector of the CUTLASS radio waves, k_r , to be directed orthogonally to the geomagnetic field vector, B_0 at the point of scatter. At high latitudes, where B_0 is near vertical, this is achievable in both the *E* and *F* regions of the ionosphere due to refraction of the radio waves. The CUTLASS radars, located at Hankasalmi (62.3°N , 26.6°E) in Finland and Pykkvibær (63.7°N , 19.2°W) in Iceland, are ideally situated to view FAIs generated by the EISCAT heater (see Figure 2).

[12] The CUTLASS Finland and Iceland radars have been operational since February and November 1995, respectively, and data from CUTLASS Finland have been used to study the patches of irregularities excited by the EISCAT heater. Both CUTLASS radars operate between 8 and 20 MHz and consist of a 16-antenna main array, which transmits and receives, and a 4-antenna interferometer array, which receives only. The degree of refraction suffered by the rays in the ionosphere is dependent upon the CUTLASS frequency as well as on ionospheric conditions. Orthogonality with Earth's magnetic field direction, therefore, occurs at different altitudes when using different CUTLASS frequencies such that different cross sections of measurement are made through the modified region of the ionosphere.

[13] During the experiments that have been studied the CUTLASS Finland frequency scanned between 18 and 19.5 MHz, and backscatter power values were provided with a 1 s time resolution. The range resolution, that is, the size of the range gates, was 15 km. Only beam 5 of the radar

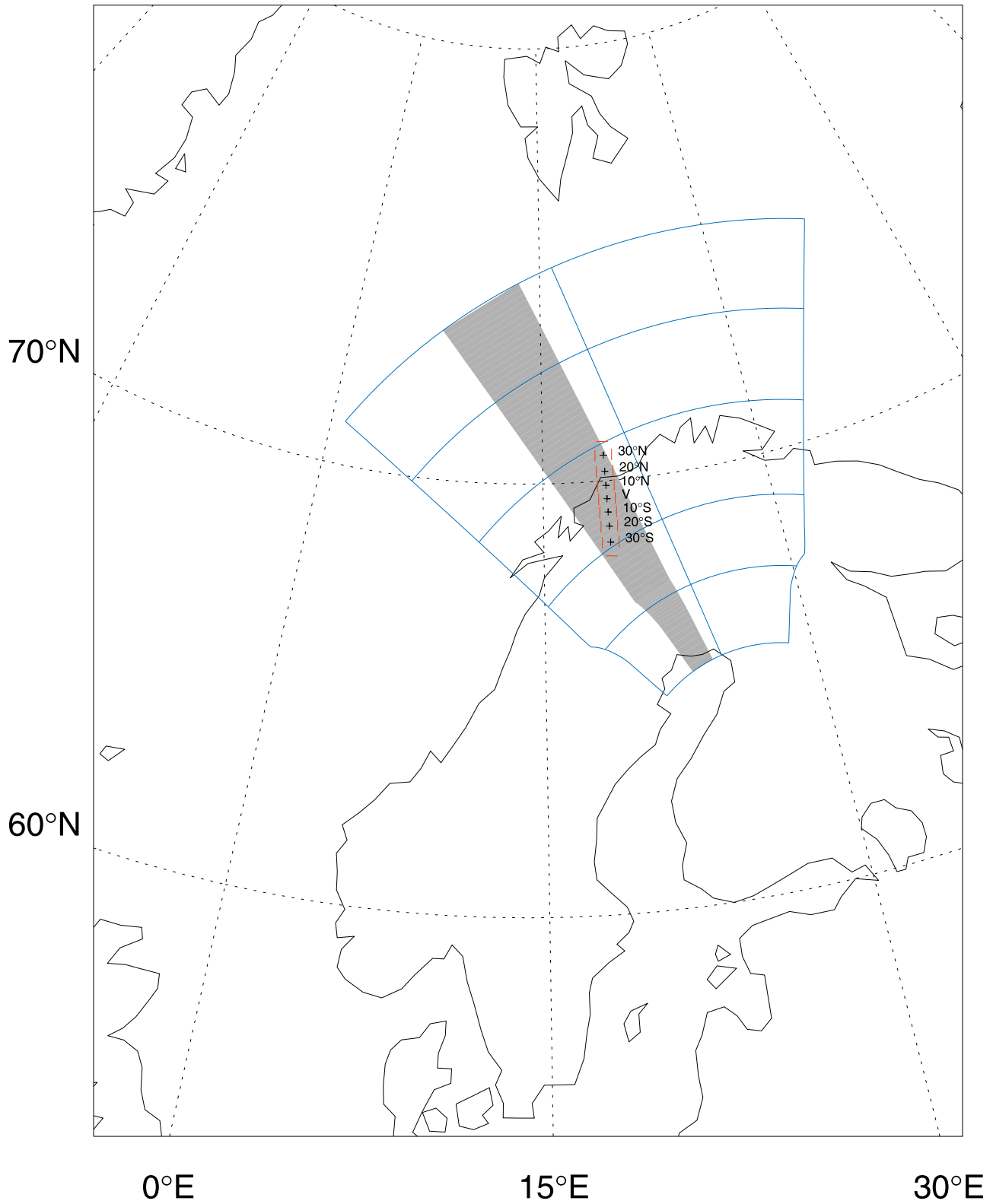


Figure 2. The field-of-view of the Co-operative UK Twin Located Auroral Sounding System (CUTLASS) Finland radar, shown as a blue outline. The gray area indicates the region covered by beam 5 of the radar, the red vertical lines indicate the 3 dB width of the heater beam while it is pointed at various directions between 30° north, vertical (V), and 30° south, and the upper and lower red horizontal lines indicate the 3 dB width of the heater beam when it is pointed 30° north and 30° south, respectively.

was in operation, and this intersects the region directly above the Tromsø heater. The distance to first range gate is 480 km in this scan mode, and 75 range gates are sampled. Analysis of the autocorrelation functions is used to derive the backscatter power, line-of-sight Doppler velocity, and spectral width. The backscatter power is the only one of the three derived parameters used in this study. In addition, results are presented from only the Finnish component of the CUTLASS pair since the Icelandic radar receives weaker and more variable backscatter powers due to the longer propagation path and the unlikelihood of achieving orthogonality with the magnetic field lines at the position of the irregularities.

[14] It is assumed that the CUTLASS rays intersect the patches of FAIs at a constant height, h_U , above the heater. This is a good approximation, given the low-angle trajectory of the radar beam at long ranges (~ 1000 km). In reality the orthogonality condition requires the rays to propagate at an angle $\theta_{B_0} = 12^\circ$ from horizontal. As is well known, the linear backscatter power measured by CUTLASS is proportional to the square of the electron density perturbation amplitudes in the ionosphere [e.g., *Schlegel*, 1996]. Thus, the CUTLASS backscatter power provides direct measurements of the mean intensity of FAI inside the scattering volume at each range.

3.3. Tromsø Dynasonde

[15] Data from the Tromsø dynasonde have been used to monitor the change in the f_oF_2 during the heating experiments. Close to the f_oF_2 the reflection altitude of the transmitted wave increases greatly with small increases in wave frequency [*Davies*, 1966]. If the frequency of a transmitted radio wave is close to the f_oF_2 , then severe refraction of the wave can occur in this area since the electron density gradient of the ionosphere is large and an electromagnetic wave is able to travel a significant distance in the horizontal direction prior to reflection. At frequencies considerably below the f_oF_2 there is a much sharper electron density boundary, and rectilinear propagation up to the reflection point is obeyed to a good approximation. Although the values of the f_oF_2 obtained from the Tromsø dynasonde did vary during the beam-sweeping runs, they remained high enough for overdense heating; therefore FAI enhancement was possible throughout the beam-sweeping runs.

3.4. EISCAT UHF Radar

[16] The EISCAT UHF radar is an incoherent scatter radar with a 933 MHz transmitter located at Tromsø and receivers at Tromsø and Kiruna, Sweden, and Sodankylä, Finland [*Evans*, 1969]. Details of the early results obtained by the EISCAT radars are given by *Rishbeth and van Eyken* [1993]. For the following investigation, electron density profiles provided by the EISCAT UHF radar were used to estimate a value of the upper hybrid height, h_U . In these EISCAT UHF data a heater-induced ionline overshoot occurs at the altitude where the plasma frequency is equal to the heater frequency, causing an apparent enhancement in the electron density [*Jones et al.*, 1986; *Rietveld et al.*, 2000]. The height difference, Δz , between this altitude level and the upper hybrid level, U , can be determined, and *Rietveld et al.* [1993] state a typical value of 6 km. The

ionline overshoots observed in the EISCAT UHF data occurred at approximately 200 km altitude during the three beam-sweeping runs. It was also found that h_U differed from this 200 km altitude by a few kilometers, and since this is much less than the CUTLASS range resolution, a value of 200 km was assumed for h_U . The upper hybrid width was thus calculated to be approximately 130 km, using equations (3) and (4).

4. Statistical Relations

4.1. CUTLASS Backscatter Power Data

[17] Each CUTLASS range gate, r , is associated with a value of linear backscatter power, p . The linear power is calculated from the logarithmic signal-to-noise ratio (p_{dB}) using

$$p = 10^{p_{\text{dB}}/10}. \quad (5)$$

If range gates $r_1, r_2, \dots, r_J, \dots$ occur with powers $p_1, p_2, \dots, p_J, \dots$, respectively, and P is the sum of the backscatter powers across all CUTLASS ranges ($\sum p_i$), then the arithmetic mean of the distribution is given by [*Spiegel*, 1972]

$$\bar{r} = \frac{\sum_{i=1}^J p_i r_i}{P} \quad (6)$$

The statistical moments of the distribution are given by

$$m_n = \frac{\sum_{i=1}^J p_i (r_i - \bar{r})^n}{P} \quad (7)$$

for $n = 0, 1, 2, \dots$. Here, m_n is the n th statistical moment about the mean. Clearly, by definition, $m_1 = 0$. In this study we utilize P and moments m_2, m_3 , and m_4 only. The variance corresponds to $n = 2$, and its square root is the standard deviation, or statistical width, σ . The skewness and kurtosis of the distribution correspond to $n = 3$ and $n = 4$, respectively. Skewness is a measure of the degree of asymmetry of a distribution such that a symmetrical distribution has a zero skewness. Kurtosis is a measure of the degree of peakedness of a distribution. The value of kurtosis gives an indication of the shape of the patch of irregularities, the kurtosis being greater for more sharply peaked distributions and for distributions with more than one peak.

[18] In the following analysis, both the skewness and kurtosis are used in their dimensionless forms. The dimensionless moments about the mean are given by

$$a_n = \frac{m_n}{\sigma^n}, \quad (8)$$

where a_n is the n th dimensionless moment about the mean and m_n is defined in equation (7). Kurtosis is probably the least familiar of the four moments dealt with, so it is worth showing some values for some familiar distributions. Table 1 shows the kurtoses of some simple symmetrical, continuous distributions. The kurtoses of the backscatter power profiles can later be compared with the kurtoses of these distribu-

Table 1. Values of Kurtosis for Some Simple Shapes

Shape	Kurtosis
Rectangular box	1.8
Parabola	2.1
Isosceles triangle	2.4
Gaussian	3.0

tions in order to get an indication of the underlying shapes of the patches.

[19] In addition to a statistical width, it is also useful to calculate a threshold width of the CUTLASS backscatter power distributions, similar to that employed by *Bond et al.* [1997]. This width provides a means of revealing the threshold pump power since the threshold width limits define the edges of a patch of irregularities where the amplitude has been raised above that of the background.

[20] The summed power of the patches of irregularities helps to determine whether the relationship between the heater beam power and the patch power is nonlinear. The mean positions and skewnesses of patches can be used to indicate the effects of changing the heater beam pointing direction and for identifying whether there is any influence on the patches from Earth's magnetic field. The widths of the patches, particularly the threshold widths, can be compared with the upper hybrid widths calculated using equations (3) and (4) in order to test the upper hybrid theory of irregularity generation. The kurtoses of the power distributions are a measure of the flatness of the patches and can be used to identify saturation of the irregularity amplitude, which is likely to produce a smaller value of patch kurtosis.

4.2. Heater Beam Model

[21] Heater beam power distributions were modeled using the EZNEC version 4 software (<http://www.eznec.com>). The distributions can be produced for any combination of heater frequency and transmitters employed during heating experiments. The software provides power distributions as a function of beam angle, α , relative to the vertical between -90° and $+90^\circ$ with a 1° resolution. The statistical moments of the heater beam power distributions as a function of the CUTLASS range can be compared directly to the moments derived from CUTLASS backscatter power data in order to examine the extent to which the local heater power density controls irregularity excitation.

[22] Statistical moments of the modeled power distributions were calculated using equations (6) to (8) and the peak position, peak power, and 3 dB half width determined using a least-squares-fit parabola to the 15 modeled data points around the maximum power provided by the software in decibels, that is, the maximum decibel power and seven modeled data points either side of this. Linear interpolation between those values that were closest to 3 dB below the peak allows the 3 dB points of the distribution to be determined.

[23] Since the CUTLASS backscatter data are provided as a function of range in kilometers, the statistical parameters of the modeled heater beam distributions must also be considered as a function of CUTLASS range rather than

beam angle. The modeled heater beam power distributions can be mapped onto U using

$$R(\alpha) = h_U \tan \alpha + R_0, \quad (9)$$

where R_0 is the range to the center of the heater beam. The values of the ERP at this altitude are calculated using

$$p(R(\alpha)) = \frac{p(\alpha)h_U^2}{h_U^2 \sec^2 \alpha}, \quad (10)$$

where $p(R(\alpha))$ is the linear ERP of the heater beam as a function of CUTLASS range and $p(\alpha)$ is the linear ERP of the heater beam as a function of angle. Mapping the distributions onto U biases the power toward the center of the distribution, resulting in slightly narrower widths.

4.3. Comparison of CUTLASS and Modeled Heater Beam Power Distributions

[24] In order to provide a guide to the meaning of the moments in the main beam, here a comparison is made between the statistical parameters of a typical heated patch and the corresponding modeled heater beam power distribution for a static, vertically pointing beam geometry (a model for the swept beam geometry will be outlined in section 6). The CUTLASS range-time-intensity (RTI) plot of a patch produced during a static, vertically directed beam transmission soon after the beam-sweeping experiments being considered is displayed in Figure 3. The corresponding backscatter power distribution of the patch is also shown, calculated by averaging the backscatter power measured in each CUTLASS range over the time period for which the heater was switched on. The dashed line shows the power distribution of the modeled heater beam. There is a good correlation between the position of the patch and the main beam.

[25] The values of the statistical parameters calculated for the patch power distribution and the modeled heater beam power distribution of Figure 3 are presented in Table 2. The statistical parameters for the beam both with and without the side lobes are provided. This was considered necessary since both the kurtosis and the statistical width of the beam are sensitive to the presence of even small side lobes and are increased in value when the side lobes are taken into account.

[26] The statistical parameters of the patch power distribution given in Table 2 match well with those of the modeled heater beam power distribution without side lobes. The mean positions of the two distributions are within a few kilometers of each other, as are the values of the statistical widths. The threshold width of the patch is significantly larger than the 3 dB width of the beam, suggesting that the beam is able to excite irregularities well outside of its 3 dB width. This is likely to be the case when the transmitted power density is well above the threshold required for FAI excitation. The skewness of the main beam is 0, indicating a symmetrical distribution, whereas the distribution of the whole beam is slightly negatively skewed, as is that of the patch. Finally, the kurtoses of the beam and patch power distributions are comparable when the side lobes of the beam are neglected. In general the statistical parameters of the patch lie between those of the main beam and those of the whole beam, the exception being the skewness of the

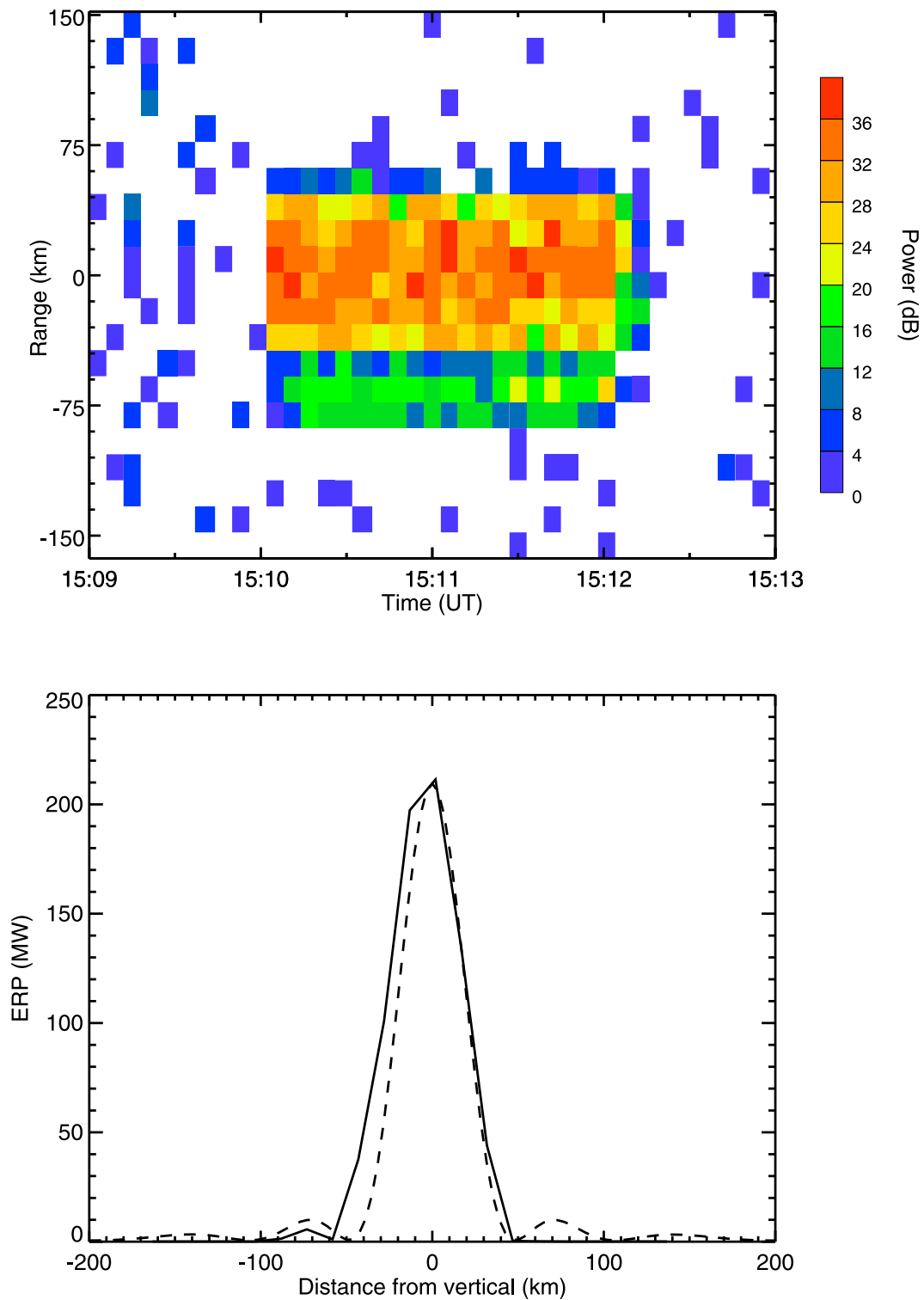


Figure 3. A CUTLASS range-time-intensity (RTI) plot of a patch created during a vertically directed heater beam transmission and the corresponding time-averaged patch power distribution. The dashed line represents the associated modeled heater beam power distribution. The patch power distribution is scaled such that the peak power matches the peak effective radiated power (ERP) of the beam.

Table 2. The Statistical Parameters Calculated for a Heated Patch Created During a Vertically Directed Heater Transmission Carried Out Immediately After Heater Beam Sweeping^a

Statistical Parameter	Beam With Side lobes	Beam Without Side lobes	Patch
Mean position (km)	-0.18	0.00	2.67
Three decibel threshold width (km)	20.73	20.73	150
Statistical width (km)	43.41	16.04	20.0
Skewness	-0.20	0.00	-0.43
Kurtosis	66.52	2.61	3.52

^aAlso shown are statistical parameters for a vertically directed modeled heater beam power distribution both with and without the heater beam side lobes.

patch, which is greater than that of the whole beam and may be an effect of Earth's magnetic field.

5. Experimental Arrangement

[27] The relationship between heater beam pointing direction and the strength of artificial FAI has been investigated by studying backscatter data measured by CUTLASS Finland during three beam-sweeping experiments carried out at the EISCAT heating facility on 6 October 1998. During each beam-sweeping run the heater power and frequency were kept fixed at 900 kW and 4.54 MHz, respectively. All 12 transmitters were used, and the beam pointing direction was made to complete a repetitive sawtooth motion. A single sweep entailed moving the beam pointing direction at a constant angular rate through 60° along the north-south geographic meridian between +30° (north) and -30° (south) from vertical. The beam then rapidly returned to the +30° position to begin the next sweep. The beam pointing was established through phasing of the antennas, and the return to the +30° pointing direction was almost instantaneous. Each of the beam-sweeping runs that have been studied spanned a 10 min interval with sweeps of 60, 10, or 1 s duration, corresponding to sweep rates of 1°, 6°, and 60° min⁻¹, respectively. A short interval at the beginning of the second beam-sweeping run consisted of sweeps of 40 s duration, and this stage was not included in the study since the period comprised only two sweeps of the beam. Details of the three periods of beam sweeping studied, labeled A–C, are given in Table 3.

[28] Observations of the heated patches made by CUTLASS and the statistical parameters of the power distributions in the patches calculated from the CUTLASS data are described in the following sections. A comparison of the CUTLASS data is made with modeled heater beam power distributions obtained from the EZNEC version 4 software in order to determine the extent to which the heater beam controls the shape, size, and position of the patches of FAIs. An explanation of the results is then discussed.

[29] The RTI plots of backscatter data obtained from CUTLASS Finland during the three beam-sweeping runs are given in Figure 4. Figure 4 (top, middle, and bottom) shows data obtained during runs A–C, respectively. In Figure 4, 0 km on the range axis represents the point along the CUTLASS beam that is vertically above the heater. This means that we set R_0 to 0. Negative ranges are toward the

CUTLASS radar, and positive ranges are farther away. The dashed horizontal lines indicate the limits of the upper hybrid width (130 km wide), and the solid horizontal lines signify the outer 3 dB points of the transmitted heater beam at the extremes of the sweeps as obtained from the EZNEC version 4 model (250 km wide). The data associated with the slowest beam-sweeping run, shown in Figure 4 (top), can be resolved into individual sweeps of 60 s duration each. High-power irregularities are observed to persist until subsequent sweeps at a range of approximately -30 km, while at all other CUTLASS ranges they rapidly disappear. This persistence was also documented by *Dhillon* [2001]. The relatively slow sweep rate employed during the short interval at the beginning of run B is visible at the left edge of Figure 4 (middle). With the exception of this region, the data for runs B and C cannot be resolved into their individual sweeps since these were of much shorter duration than the sweeps of run A and are comparable with the CUTLASS time resolution. Data in Figure 4 (bottom), associated with run C, show two distinct bands of high-power irregularities from 1456:00 UT onward, lying close to CUTLASS ranges of +45 and -45 km. Prior to this time only one band of irregularities was present. The data in Figure 4 are positioned approximately symmetrically about 0 km, extending to just beyond the upper hybrid width limit in both directions and remaining well within the regions swept out by the heater beam.

6. Analysis

6.1. Heater Beam Model

[30] Before we present the results of the statistical moment analysis of the CUTLASS intensity distribution data, we outline the power distribution of the modeled heater beam during the beam sweeps. Heater beam power distributions as a function of beam angle have been modeled using the EZNEC version 4 software for the heater frequency and transmitters employed during the beam-sweeping experiments. A modeled heater beam power distribution has been produced for heater beam transmission angles, θ , between 0° and -30° from vertical, inclusively. It is assumed that the power distributions are symmetrical about the vertical beam pointing direction, so it is unnecessary to calculate power distributions for θ lying between +1° and +30°. Figure 5 displays the modeled power distributions for heater beam transmission angles between 0° and -29°. The dotted lines represent the limits of the upper hybrid width, which are positioned symmetrically about $\alpha = 0$. As the heater beam pointing direction moves farther from vertical, the position of the main beam shifts toward the left side of Figure 5, toward negative values of α , and the magnitude and number of side lobes toward the right side of Figure 5

Table 3. Details of Beam-Sweeping Runs Carried Out at the European Incoherent Scatter Heating Facility on 6 October 1998

Run	Time (UT)	Duration of Each Sweep (s)	Number of Sweeps
A	14:30:00–14:40:00	60	10
B	14:43:43–14:52:03	10	50
C	14:54:00–15:04:00	1	600

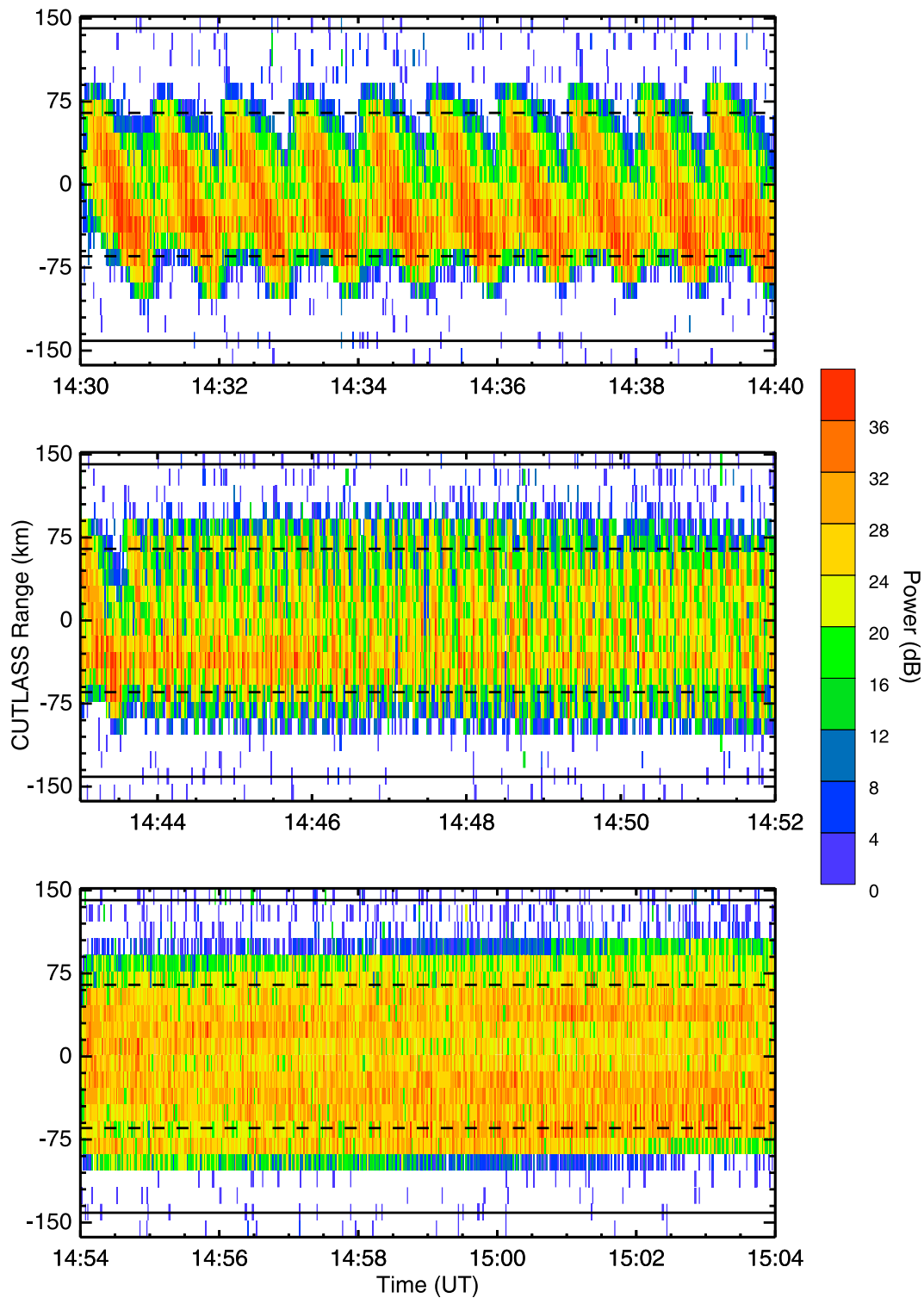
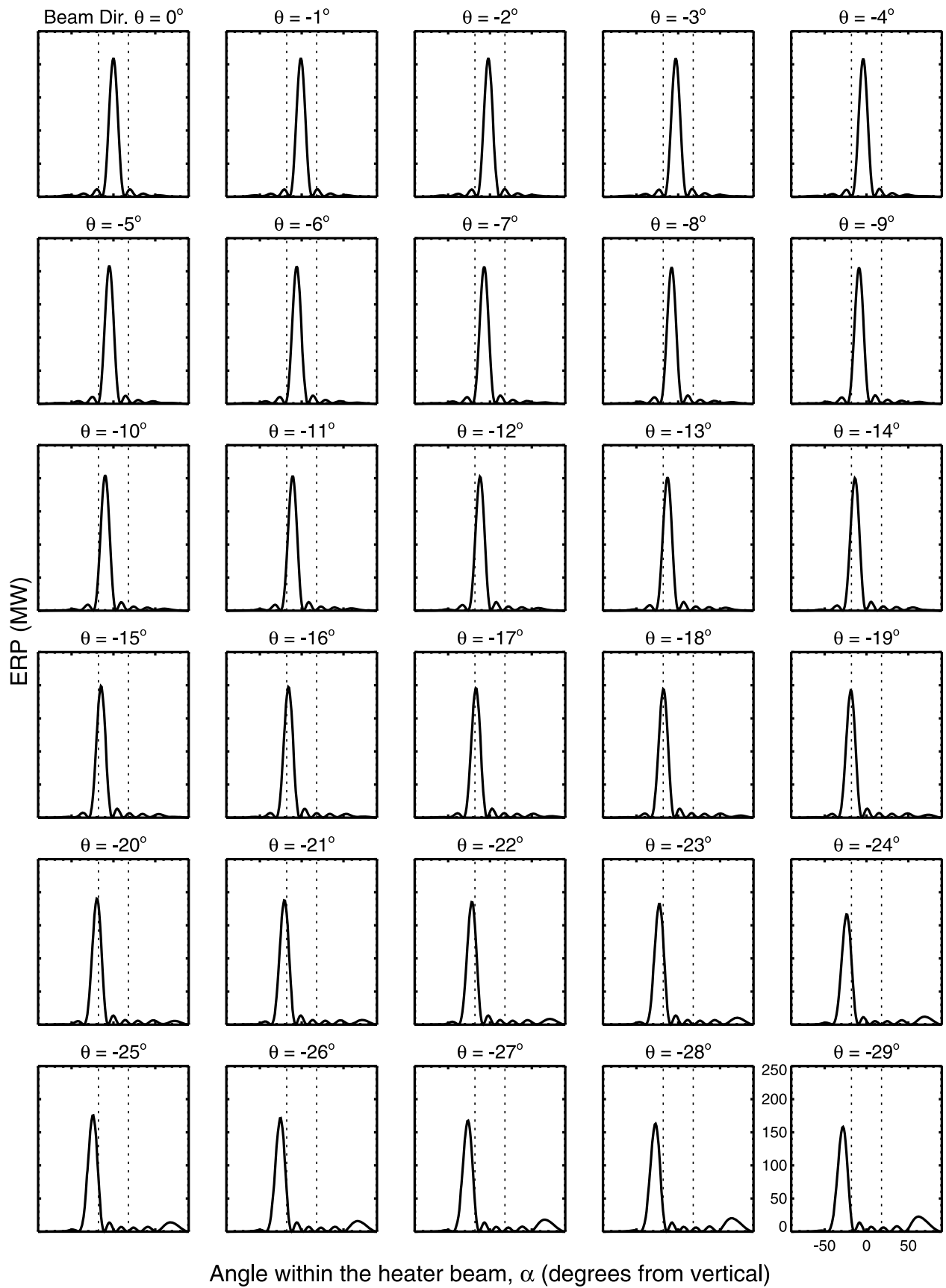


Figure 4. CUTLASS RTI plots showing the backscatter power measured during 60, 10, and 1 s beam-sweeping experiments. The dashed lines indicate the upper hybrid width limits, and the solid lines indicate the positions of the 3 dB points of the heater beam at the extremes of the sweeps. The slower sweep rate at the beginning of the second run is evident in Figure 4 (middle).

increases. The statistical moments, peak position, peak power, and 3 dB half width of each of these distributions can be calculated as described in section 4.2. For the heater beam power distributions corresponding to $\theta = \pm 23^\circ$, two

equal-valued maximum powers were provided by the beam-modeling software, so in this case both of these points and seven points either side of them were used for the fitting of the parabola.



Angle within the heater beam, α (degrees from vertical)

Figure 5

[31] Figure 6 (top) displays the summed power (Figure 6a), mean position (Figure 6b), 3 dB half width (Figure 6c), statistical width (Figure 6d), skewness (Figure 6e), and kurtosis (Figure 6f) of the modeled beam power distributions as they vary with heater beam transmission angle. Figure 6 (bottom) displays these same parameters for the power distributions without the side lobes, which were removed by cutting off the heater beam power distributions at the values of α where the first minima in linear power occur at either side of the main beam.

[32] There is a drop in power when the heater beam is pointed farther from vertical, observed in Figure 6a (top), since there is a greater distance from the heater to U for larger angular displacements of the heater beam.

[33] The dashed lines in Figure 6b (top, bottom) represent equality between the position of θ when projected onto U and the range along the CUTLASS beam from R_0 in this plane. The mean beam position matches the line when only the main heater beam is taken into account, as in Figure 6b (bottom). It is evident that the effect of the side lobes is to cause the mean position of the heater beam to deviate from the line toward the vertical direction, particularly when the angular displacement of the beam from vertical is greater, when the side lobes are at their most powerful and most numerous.

[34] The variations of the 3 dB half width with transmission angle, shown in Figure 6c (top, bottom), are identical since in both cases it is the half width of the main beam that is considered, independent of the side lobes. The 3 dB half width increases between heater beam transmission angles of 0° and $\pm 30^\circ$, but by less than 10 km. Since the CUTLASS Finland radar has only a 15 km resolution, a 10 km change in patch width would not be resolved. A similarly small increase of less than 10 km is observed in the statistical width of the main beam in Figure 6d (bottom) between $\theta = 0^\circ$ and $\pm 30^\circ$. The statistical width in Figure 6d (top) displays a large 80 km increase between heater beam transmission angles of 0° and $\pm 30^\circ$, as a consequence of the beam side lobes. The side lobes, which are small for vertical pointing of the heater beam, become larger with increasing angular displacement from vertical, resulting in a larger statistical width of the power distribution. However, the presence of even the small side lobes at $\theta = 0^\circ$ produces a statistical width of almost 40 km, which is considerably larger than the approximate 20 km statistical width of the main beam.

[35] The power distributions in Figure 5 become less symmetrical as the heater beam is pointed farther from vertical, mainly due to the change in the side lobes. When the beam points in the negative direction, as is the case for the power distributions displayed in Figure 6, the side lobes are on the positive side of the main beam and the skewness becomes more positive as θ becomes more negative. Conversely, for positive angular displacements (not shown), the side lobes are on the negative side of the main beam and these distributions have a negative skewness. This change in

skewness is observed in Figure 6e (top) until an angular displacement of approximately 20° from vertical. Beyond this, the magnitude of the skewness decreases as the number of side lobes remains steady and their power increases, thus making them more comparable in size with the main beam, which decreases in power. Figure 6e (bottom) indicates that the main beam without side lobes is actually skewed in the opposite direction. The magnitudes of skewness of the main beam distributions are relatively small, so the distributions are effectively symmetrical.

[36] The main beam power distributions in Figure 5 are slightly sharper for greater angular displacements of the heater beam from vertical, as deduced from the increasing kurtosis with increasing transmission angle in Figure 6f (bottom). The increase in kurtosis is less than 0.5, and the main beam powers resemble a flattened Gaussian distribution. The relatively large values of kurtosis observed in Figure 6f (top) are a consequence of the multi peaked nature of the full beam since this statistical moment is very sensitive to noncomparable peaks within a distribution. At angular displacements of the beam that are greater than 20° the kurtosis rapidly decreases as the number of beam side lobes stops changing and their growth, together with a decrease in strength of the main beam, results in a flatter distribution.

6.2. CUTLASS Data

6.2.1. Run A: Slowest Beam Sweeps

[37] The statistical parameters calculated from the CUTLASS data corresponding to beam-sweeping run A are plotted against time in Figure 7. Vertical lines indicate the beginning of each sweep when the heater beam pointing direction was changed from -30° (southward) to $+30^\circ$ (northward). The horizontal line in Figures 7a and 7c indicates the position vertically above the heater, and the dashed horizontal line in Figure 7d indicates the value of the upper hybrid width calculated using equations (3) and (4).

[38] Notice that the summed power of the patch, shown in Figure 7b, increases and decreases with time as the heater beam transmission angle varies between $+30^\circ$ (northward) and -30° (southward). During the first few sweeps of the beam the summed power peaks close to when the heater beam is pointed vertically, in the middle of the sweep. For later sweeps, however, the peak of the summed power occurs approximately halfway through the southward pointing half of the sweep.

[39] The mean position of the patch of FAIs, shown in Figure 7c, varies between slightly positive and negative ranges as the heater beam direction is moved from northward to southward pointing. Apart from the results of the first beam sweep, which show a maximum mean position of 40 km occurring approximately 5 s after the start of the sweep, the most positive mean patch position of 20 km occurs approximately 15 s after the start of each sweep. The most negative mean patch position of -50 km occurs very close to when the heater beam is pointed in its most

Figure 5. Heater beam power distributions, as a function of angle, produced by the EZNEC version 4 software for an azimuth of 180° . A distribution is displayed for beam pointing directions between 0° and -29° from vertical at 1° resolution. The pointing direction of the heater beam is given for each case, and the dotted lines indicate the limits of the upper hybrid width.

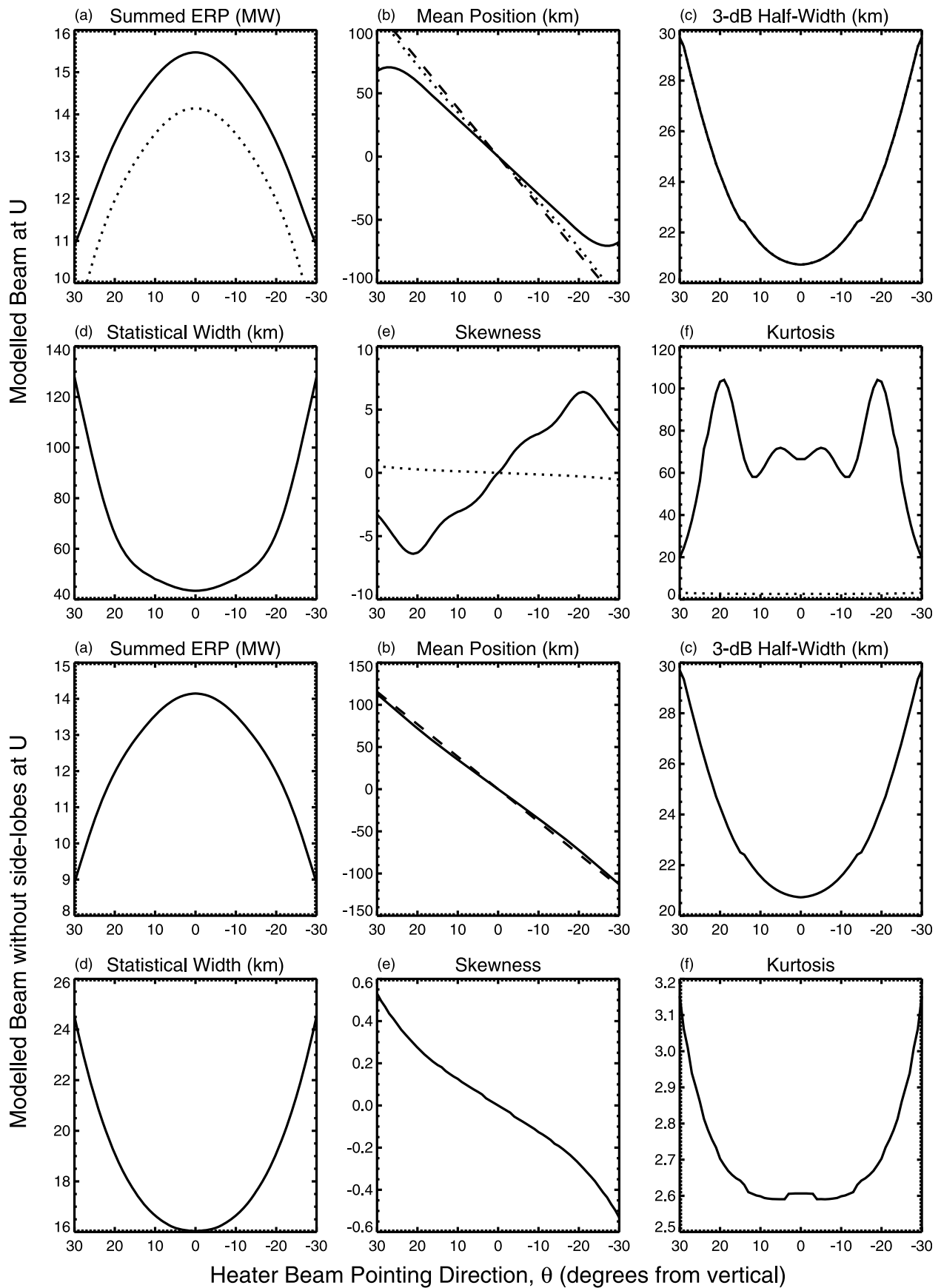


Figure 6

southward direction for all sweeps. During earlier sweeps the mean position of the patch lies vertically above the heater when the heater beam is pointed vertically, at the center of the sweep. During later sweeps the mean position of the patch lies vertically above the heater a few seconds after the heater beam is pointed vertically. Clearly there is a large bias of mean position toward negative values despite the apparent symmetrical placement of the patch about 0 km, which is observed in the CUTLASS RTI plot in Figure 7a. This bias is due to the effect of the strong, persisting irregularities positioned close to -30 km.

[40] The threshold width of the patch, displayed in Figure 7d, takes values close to 200 km at the start of each sweep with the exception of the first. It then rapidly decreases to approximately 150 km, remaining at this value for the second half of each sweep. These values of threshold width are much smaller than the 250 km width swept out by the heater beam. However, the steady 150 km value of threshold width lies close to the 130 km value of the upper hybrid width calculated using equations (3) and (4). The statistical width, calculated from equation (7), is also relatively large close to the beginning of each sweep before decreasing to a steady value of 20 km, which is retained during the second half of the sweeps. For the first 10 s of each sweep, as θ changes from $+30^\circ$ to $+20^\circ$, the statistical width increases from 20 km to a maximum value of approximately 30 km in the first sweep and 50 km in the final few sweeps.

[41] For the first 20 s of each sweep the skewness, shown in Figure 7f, is observed to decrease, taking a minimum value after this time. For sweeps earlier on in the run the decrease is from $+1$ to -1 , later becoming a decrease from $+2$ to -1 . Between 20 and 45 s after the start of each sweep, the skewness increases to positive values of approximately $+1$ again. The patch tends to become positively skewed slightly before the middle of the sweep, passing the point of symmetry while the heater beam is still directed northward. After 45 s from the start of the sweeps, the skewness decreases again, and in some cases becomes negative, before a rapid increase to $+1$ or $+2$ as a new sweep begins.

[42] The kurtosis of the patch, displayed in Figure 7g, decreases to a value of approximately 2 within the first 10 s of each sweep, from values of around 8 for sweeps at the beginning of the run to 10 for sweeps toward the end of the run. There is then a slow rise in kurtosis, up to a value of approximately 6. After 45 s from the start of the sweeps, the kurtosis decreases to values of 2–3 before rising sharply as a new sweep begins.

6.2.2. Run B: Intermediate-Rate Beam Sweeps

[43] Figure 8 displays the time dependence of the statistical parameters of CUTLASS data associated with beam-sweeping run B after a running average was performed. The CUTLASS data had a time resolution of 1 s, and the running average involved calculating the mean power of each set of three consecutive power values in order to reduce noise. The point vertically above the heater is again indicated in Figures 8a and 8c by a horizontal line, and the mean value

of each statistical parameter is plotted as a dotted line. Since the CUTLASS time resolution was 1 s, during which the heater beam moved through 6° , the variation of the statistical parameters during any one sweep could not be determined to as great an accuracy as for run A, so only a description of the overall variation of the parameters is given here.

[44] All statistical parameters display a periodic dependence on time, with a variable amplitude and median value. The amplitude and median value of the summed patch power decrease with time as the run progresses. The mean patch position is more consistent, varying between $+20$ and -40 km during each sweep. The threshold width of the patch also remains steady, with a very small, approximately 25 km, amplitude of variation. A relatively large 200 km value is observed rather than the 150 km of run A. The statistical width consistently varies between 50 and 30 km. The patch skewness varies between 0 and $+2$ during earlier sweeps and between -1 and $+1$ toward the end of the run. The kurtosis displays a similar change, varying between 2 and 7 during earlier sweeps and between 2 and 4 during later sweeps.

6.2.3. Run C: Fastest Beam Sweeps

[45] During the fastest beam sweeps, run C, when θ was changed from $+30^\circ$ (northward) to -30° (southward) in 1 s, the transmitted heater beam formed an effective power distribution, wider than a stationary heater beam distribution. Figure 9a displays the power profile of a modeled “virtual” beam created from a superposition of the individual power profiles provided by the software after modifying those corresponding to $\theta = 0^\circ$ and -24° . This was produced by summing the power values associated with a particular value of α for each of the beam pointing directions between $+30^\circ$ and -30° and dividing by the number of pointing directions. The power profile has been projected onto U using equations (9) and (10), and the dashed lines indicate the upper hybrid width limits. Figure 9b shows the distribution produced after superposition of the individual power profiles without their side lobes. Table 4 displays the statistical moments of these effective power distributions. Clearly the statistical widths of the two distributions are comparable, while the kurtoses take very different values. The relatively large value of kurtosis of beam (a) is noninformative since this is due to the irregular shape of the distribution caused by the heater beam side lobes. The value of kurtosis of beam (b) is comparable with those of the observed heated patches, while it is meaningless to make a comparison between the heated patches and beam (a).

[46] Figure 10 displays the statistical parameters of CUTLASS Finland data measured during the beam sweeps commencing at 1454:00 UT (run C). As with runs A and B, a running average was performed on the CUTLASS data prior to carrying out the calculations. Again, the horizontal dashed line in Figure 10d indicates the size of the upper hybrid width and the horizontal solid line in Figures 10a and 10c indicates the position vertically above the heater. The mean value of each statistical parameter is again plotted as a

Figure 6. Variation of (a) summed power, (b) mean position, (c) 3 dB half width, (d) statistical width, (e) skewness, and (f) kurtosis of the modified modeled heater beam power distributions with transmission angle at a height h_U (top) with and (bottom) without the beam side lobes. For comparison, the dotted lines in Figure 6 (top) indicate the values of the parameters in Figure 6 (bottom).

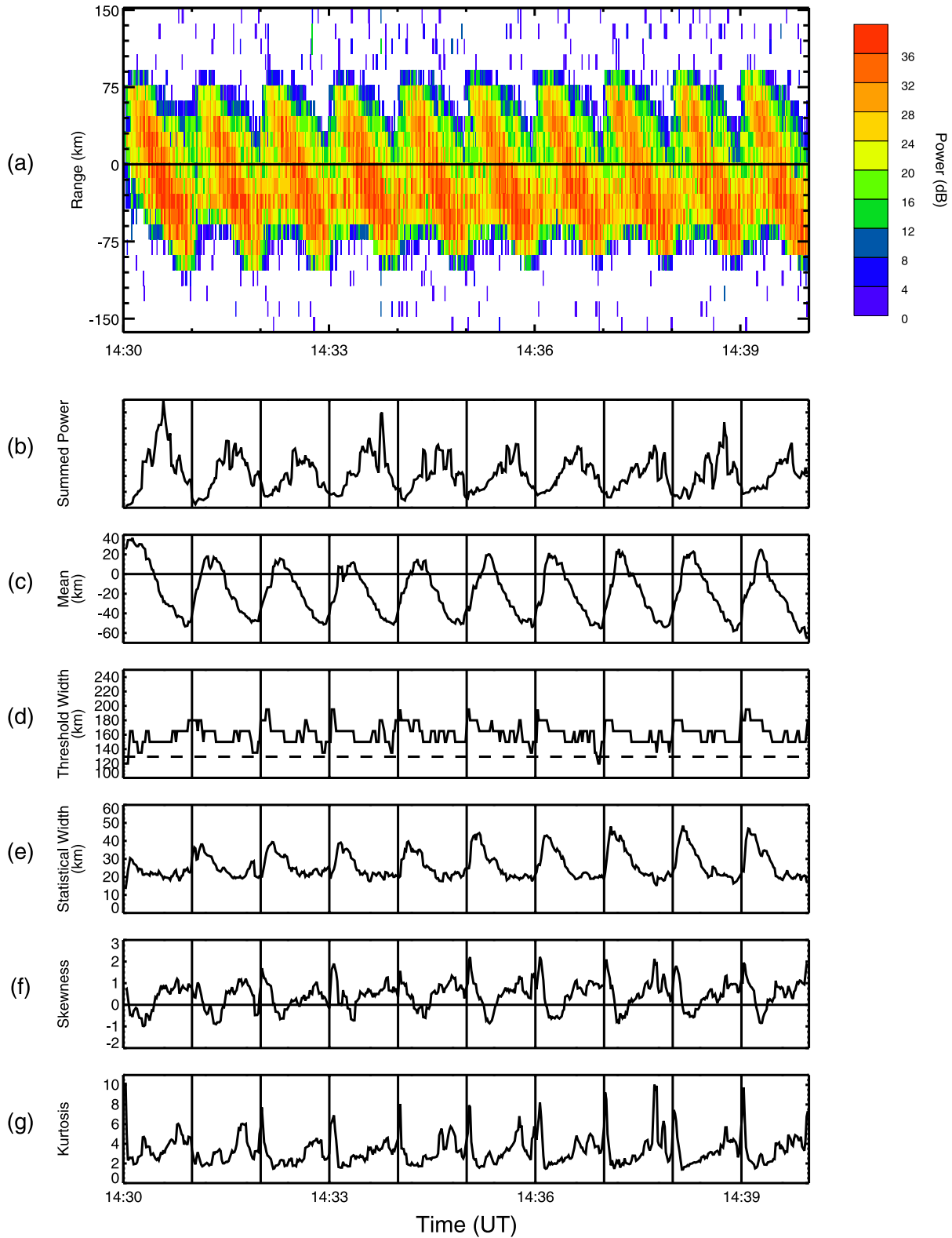


Figure 7. Variation of the statistical parameters of CUTLASS data measured during beam-sweeping run A. Vertical lines indicate the beginning of each sweep, and the horizontal dashed line in Figure 7d represents the upper hybrid width. The horizontal line in Figure 7a indicates the position vertically above the heater.

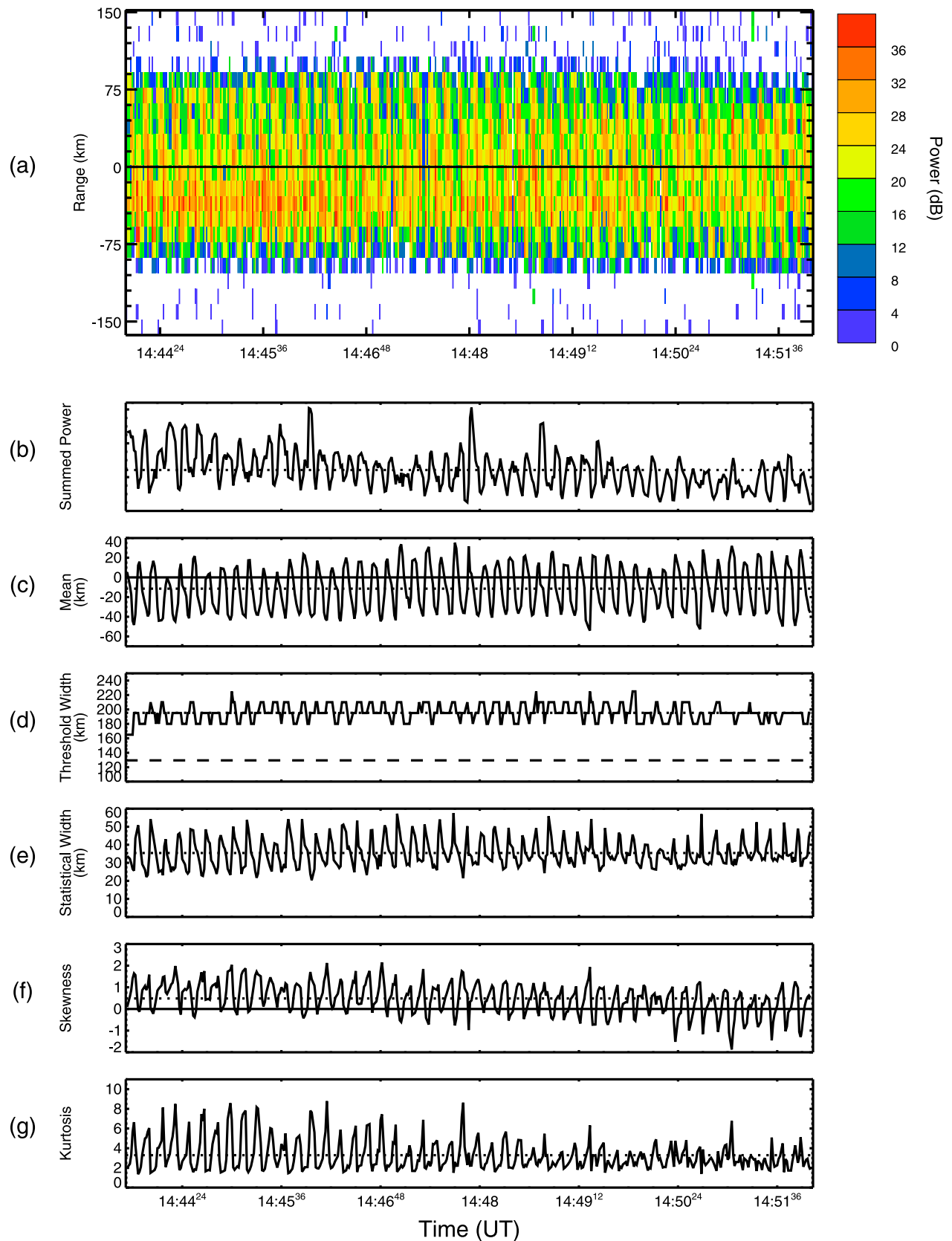


Figure 8. Variation of the statistical parameters of CUTLASS data measured during beam-sweeping run B. The dotted lines indicate the mean values of these parameters, the horizontal dashed line in Figure 8d represents the upper hybrid width, and the horizontal line in Figure 8a indicates the position vertically above the heater.

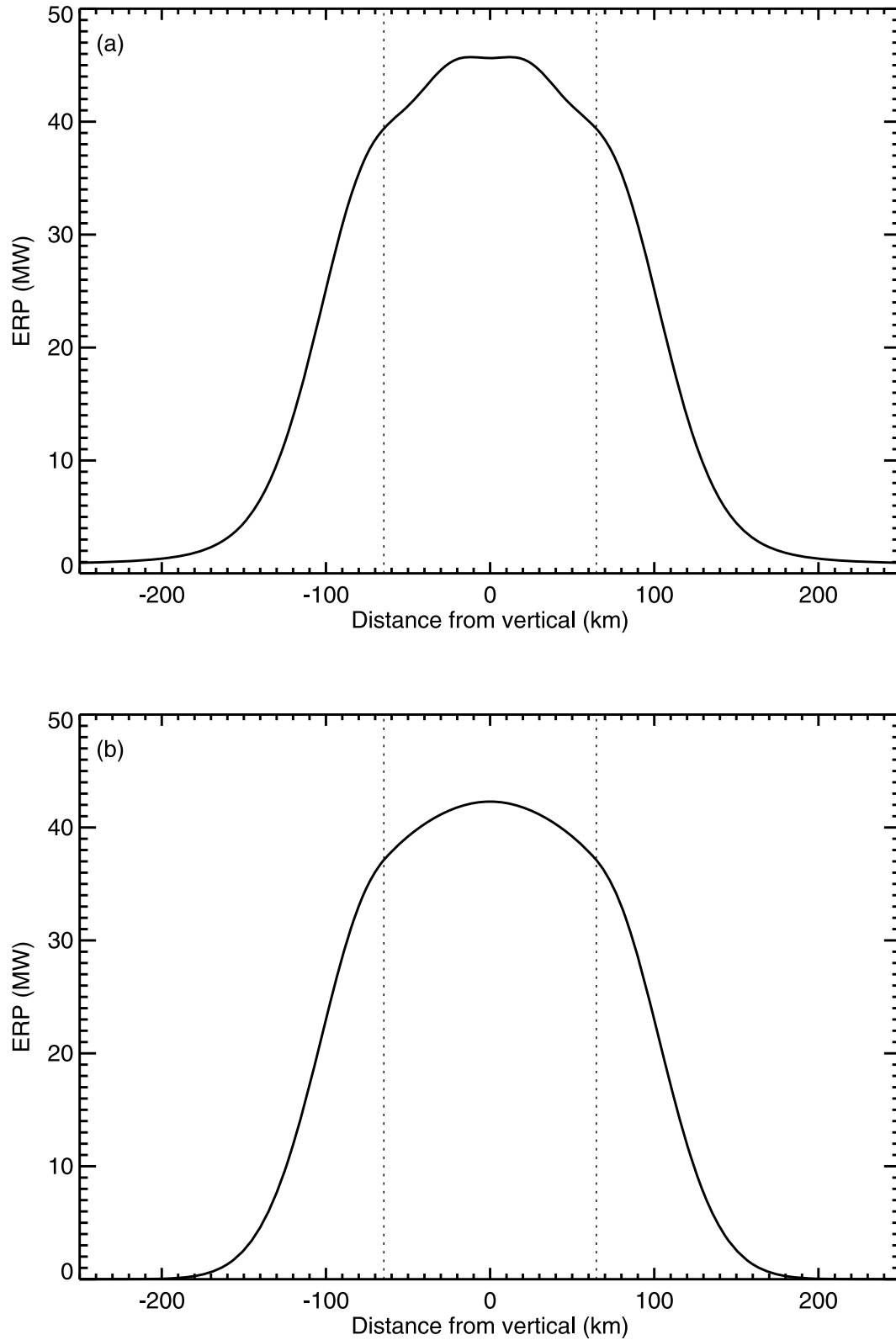


Figure 9. Superposed modeled heater beam power distributions produced by summing those shown in Figure 5 (a) with and (b) without the beam side lobes. This may represent the power distribution in the transmitted heater beam during fast beam sweeps. The dashed lines indicate the limits of the upper hybrid width. The statistical moments for these distributions are given in Table 4.

Table 4. Statistical Moments of the Modeled Beam Power Distributions in Figure 9

Statistical Moment	With Side lobes	Without Side lobes
Mean (km)	0.00	0.00
Statistical width (km)	81.84	63.24
Skewness	0.00	0.00
Kurtosis	27.87	2.33

dotted line, and the green lines indicate the values of the statistical moments of the modeled virtual beam summed without the side lobes. The mean position and skewness of the modeled virtual beam summed with the side lobes are equal to those of the modeled virtual beam summed without the side lobes; however, the statistical width and kurtosis values are much greater and are not visible on the scales in Figure 10. The values of the statistical parameters for the modeled virtual beam summed with and without the side lobes are displayed in Table 4. The CUTLASS statistical parameters in Figure 10 show roughly constant values throughout the run, although both the summed power and skewness of the patch increase slightly as the run progresses.

[47] Figure 11a displays, in decibels, the modeled virtual beam power distribution, summed without side lobes, and averaged CUTLASS Finland backscatter power profiles calculated for each of the three beam-sweeping runs. The positions of the vertical and magnetic field directions are indicated by solid and dot-dashed vertical lines, respectively, and the upper hybrid width limits are indicated by dotted vertical lines. The three CUTLASS power distributions in Figure 11a are roughly parabolic, although the distributions from runs A and B display an additional peak in the magnetic field direction, while the distribution from run C shows a dip of a few decibels in the vertical direction. It is clear that the virtual beam power distribution Figure 11a is much wider than the CUTLASS backscatter power distributions.

[48] Figure 11 summarizes and compares the values of mean position (Figure 11b), threshold width (Figure 11c), statistical width (Figure 11d), skewness (Figure 11e), and kurtosis (Figure 11f) of the mean linear backscatter power distributions of all three runs and the statistical moments of the virtual beam power distribution. It is apparent from Figure 11 that the statistical moments of patches created during beam-sweeping runs C and B are more comparable with the statistical parameters of the virtual beam than are those from beam-sweeping run A, suggesting that these faster beam sweeps, and particularly run C, have an effect that is similar to that of a wider-than-usual heater beam. The virtual beam is symmetrical, with a mean position of zero, while the CUTLASS data are positively skewed and have negative mean positions. The mean position of the patch created during run A is between 10 and 15 km closer to CUTLASS than the mean positions of patches created during runs B and C, and is least comparable with the mean position of the virtual beam distribution. The most symmetrical CUTLASS power profile is that of run C, with a skewness of 0.2. The two CUTLASS power profiles associated with runs A and B have greater skewnesses, close to 0.5 and 0.6. The threshold widths of the three backscatter power distributions are within a range gate of each other, with those corresponding to runs B and C being 210 km and

that to run A being 195 km. The dotted line indicates the size of the upper hybrid width. The statistical widths of the CUTLASS distributions are larger for faster sweep rates and are evenly separated by 6–7 km. The largest statistical width, associated with data from run C, is approximately 47 km and is 15 km smaller than the statistical width of the virtual beam. The kurtoses of the CUTLASS distributions are also evenly spaced, with comparable values between approximately 1.9 and 2.8. The kurtosis of the virtual beam resembles that of the power distribution measured during run B.

[49] FAIs produced during run C can be compared with those produced during steady vertical heater transmissions to determine the effect of the essentially wider transmitted heater beam. Figure 12a displays CUTLASS backscatter power profiles, in decibels, corresponding to data averaged over the duration of run C and over four periods of 2 min duration each (1–4) when the heater transmitted vertically. Transmissions 1 and 2 followed immediately after run C, and transmissions 3 and 4 were carried out 1 h later. During the first vertical transmission the CUTLASS frequency scanned between 18 and 19.5 MHz with a time resolution of 1 s, as during the beam-sweeping runs. Thereafter the CUTLASS frequency was 19.5 MHz with a time resolution of 6 s. The power distributions of the modeled vertical beam without side lobes and the virtual beam summed without side lobes are also shown in Figure 12a, in decibels. Figure 12a indicates that, on average, the patch power during run C spanned a wider area and was smaller in amplitude than that during the vertical transmissions, despite the same heater power setting. The virtual beam distribution is much wider than the CUTLASS power profile associated with run C, while the modeled vertical beam distribution is comparable with the CUTLASS power profiles associated with the vertical transmissions.

[50] Figures 12b–12f show the values of the statistical parameters of the mean linear backscatter power distributions, and the modeled virtual and vertically transmitted beam distributions, without side lobes. The statistical width of the CUTLASS data measured during run C is more than 20 km greater than the widths of data measured during the vertical heater transmissions. The threshold width is also greater. The other statistical moments take a range of values during the vertical transmissions, and the corresponding values for data from run C are not notably dissimilar. The statistical width of the modeled vertical beam distribution shows good agreement with the widths of the CUTLASS data measured during the vertical transmissions. The statistical width of the virtual beam power distribution is much larger than these and more comparable with that of CUTLASS data measured during run C. The skewnesses and the kurtoses of the two modeled distributions lie within the corresponding range of values taken by the CUTLASS power distributions.

7. Discussion

[51] The CUTLASS Finland backscatter power profiles obtained during the 10 heater beam sweeps of run A carried out between 14:30:00 and 14:40:00 UT were averaged over the heater beam pointing directions to produce a mean power profile for each pointing direction between +30°

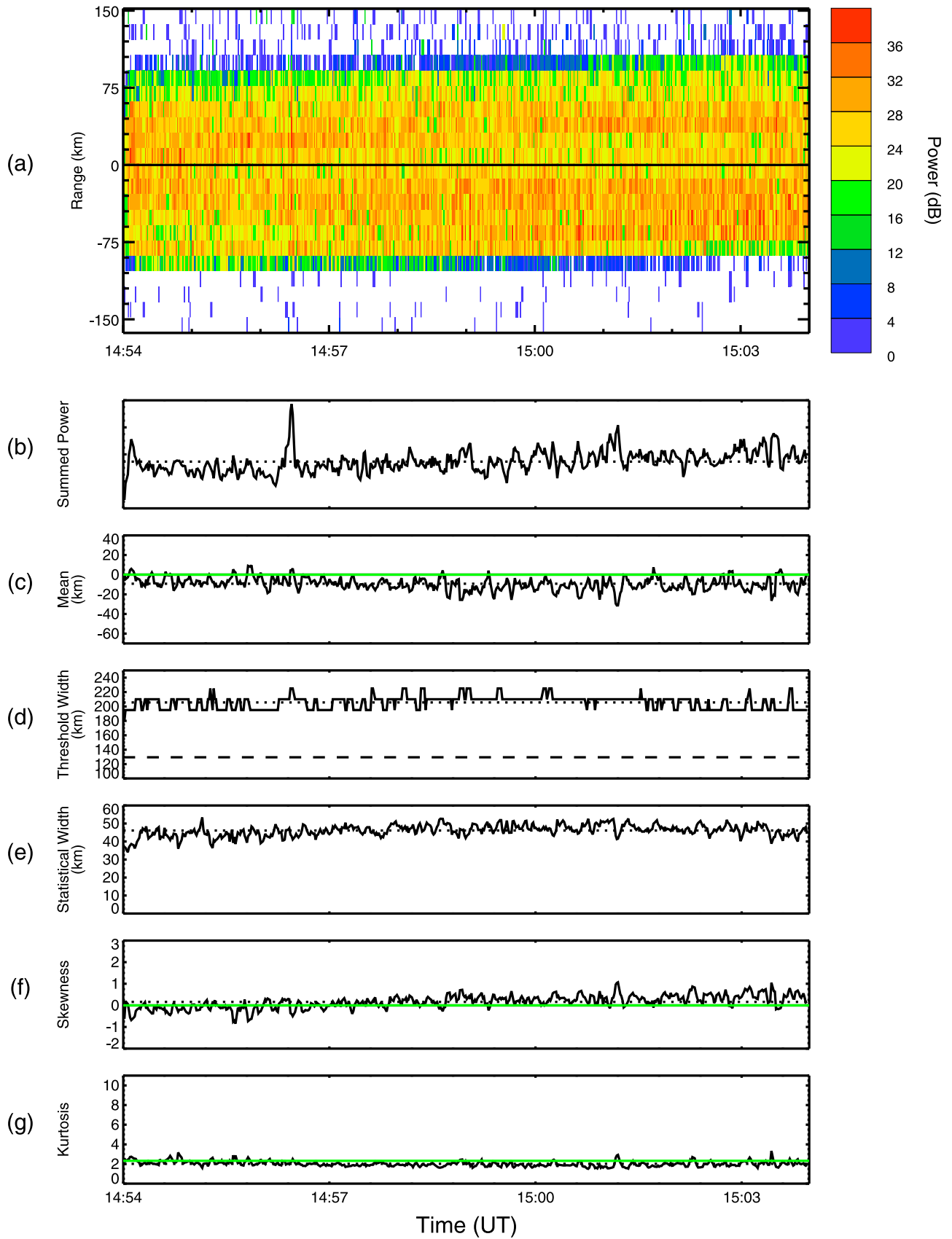


Figure 10

(northward) and -30° (southward) at 1° resolution. The averaged linear backscatter power distributions are plotted in Figure 13 together with the modeled heater beam power distributions (dotted lines) as a function of range along the CUTLASS beam. Both sets of distributions are scaled to have a common arbitrary maximum. The solid, dot-dashed, and dotted vertical lines in Figure 13 indicate the vertical and magnetic field directions and the upper hybrid width limits, respectively. The heater beam transmission angle is given in the top left of each panel.

[52] The backscatter powers are smaller during positive heater beam transmission angles than during the equivalent negatively pointed directions, and the largest backscatter powers were measured when the heater beam pointed close to the field-aligned direction. *Rietveld et al.* [2003] also observed a bias of backscatter power in the magnetic field direction and relatively large EISCAT UHF electron temperature enhancements during experiments involving 8 min heater transmissions in the 0° , -6° , and -12° pointing directions. *Rietveld et al.* suggested self-focusing effects to explain the bias [*Bernhardt and Duncan*, 1982] whereby the heater beam rays are refracted by the field-aligned ionospheric electron density depletions, resulting in higher heater powers in this direction.

[53] In Figure 13, between $\theta = 30^\circ$ and 25° , irregularities are present near the magnetic field direction but not in the vicinity of the main heater beam. These are observed to decay, although not completely, and correspond to irregularities positioned at approximately -30 km in Figure 4. Since decay of FAIs can take up to a few minutes [e.g., *Bond*, 1997; *Robinson et al.*, 1998], while the time for each heater beam sweep is only 1 min, these irregularities are likely to be a residual effect of the previous sweep. It is also possible, however, that the irregularities are a result of power transmitted through side lobes of the heater beam. It would therefore be of benefit to repeat the experiment with a delay between sweeps in order to allow the irregularities to decay completely and determine whether the side lobes of the heater beam are exciting the irregularities near the magnetic field direction.

[54] At $\theta = 24^\circ$ in Figure 13 irregularities begin to appear just within the upper hybrid width limit, as the main heater beam enters this area, while those present in the magnetic field direction remain, producing a double-peaked backscatter power distribution. Between $\theta = 24^\circ$ and 15° the patch of irregularities in the vicinity of the main heater beam grows as more of the main beam enters the upper hybrid width region. The irregularities in the magnetic field direction continue to decay, and the patch remains almost completely within the upper hybrid width limits. Between $\theta = 14^\circ$ and 6° the two sets of irregularities merge as it appears the decaying irregularities become reexcited by the heater beam. Between $\theta = 6^\circ$ and -17° (southward) the patch moves toward more negative ranges as the heater beam traverses the region within the upper hybrid width limits. Beyond a transmission angle of -17° the irregularities begin

to decay as the beam leaves the upper hybrid width region. Again, the patch does not extend very far beyond the upper hybrid width limit. Figure 13 provides compelling evidence in support of the upper hybrid model of FAI excitation since, despite the significant powers when the heater beam is pointed at large angular displacements from vertical, FAIs are not excited outside of the upper hybrid width limits. A further point to note is that as the heater beam sweeps through the local meridian plane it moves obliquely through the CUTLASS beam, as indicated in Figure 2. The CUTLASS beam is oriented at approximately 27.5° to the meridian plane; however, the modeled CUTLASS beam width is sufficiently large so as not to affect the visibility of any irregularities that would be produced at the extremes of the heater sweep. Thus the absence of irregularities observed at these extreme positions is still most likely to be because of the upper hybrid limitations described above.

[55] Figure 14 displays the data from Figure 13 in a form similar to Figure 4 but with the heater beam pointing direction along the abscissa rather than the time. The solid, dashed, dot-dashed, and dotted lines in Figure 14 indicate the position vertically above the heater and the positions of the peaks of the modeled heater beam power distributions, the magnetic field direction, and the upper hybrid width limits, respectively. Since the heater transmits symmetrically either side of vertical, it is expected that the patches should be positioned symmetrically about 0 km, as observed here, and again the placement of the patch within the upper hybrid width limits is evident. The larger powers measured during negative heater beam transmission angles are also visible. It is clear that the aforementioned double-peaked structure is likely to be caused by the presence of irregularities from the preceding sweep close to -30 km, in addition to the irregularities created by the new sweep close to 60 km along the CUTLASS beam from the point vertically above the heater. These persisting FAIs were identified in section 5 when we presented the CUTLASS RTI plots of data from the three beam-sweeping runs. *Dhillon* [2001] suggested that the persistence of the irregularities may have been caused by either a wide heater beam that constantly transmitted high powers in the central area, even when pointed far from this direction, or a significantly higher power in the center of the vertically pointed heater beam such that this region received a greater heater power than all others, leading to a greater FAI amplitude. It appears here, however, that the higher-powered regions are not positioned centrally but lie close to the magnetic field direction. It has already been established that irregularities tend to be of a higher power in the magnetic field direction. As mentioned, decay of FAIs can take up to a few minutes, and, therefore, these persisting irregularities may be decaying and taking longer to decay than others because of their initial high amplitude.

[56] Figure 15 displays the statistical parameters of the backscatter power data in Figure 14. Dotted lines in Figure 15 indicate the statistical moments of the modeled heater beam power distributions without side lobes at U , as

Figure 10. Variation of the statistical parameters of CUTLASS data measured during beam-sweeping run C. The dotted lines indicate the mean values of these parameters, and the statistical moments of the power distribution in Figure 9b are shown in green. The horizontal dashed line in Figure 10d represents the upper hybrid width, and the horizontal line in Figure 10a indicates the position vertically above the heater.

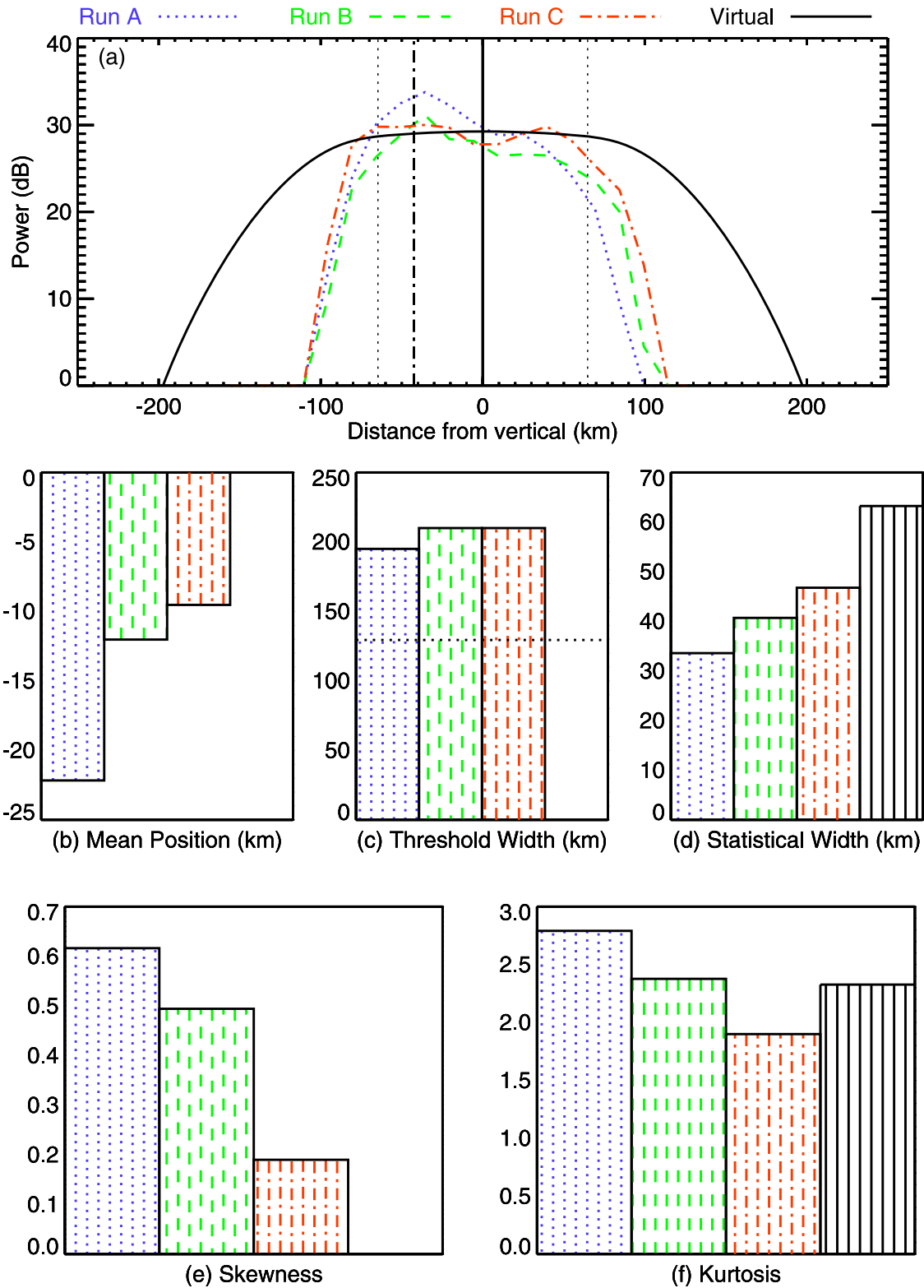


Figure 11. (a) The virtual beam power distribution of Figure 9b and the mean of the CUTLASS backscatter power distributions measured during the three beam-sweeping runs, in decibels, and (b) mean position, (c) threshold width, (d) statistical width, (e) skewness, and (f) kurtosis of the linear virtual beam power distribution and mean linear backscatter power distributions.

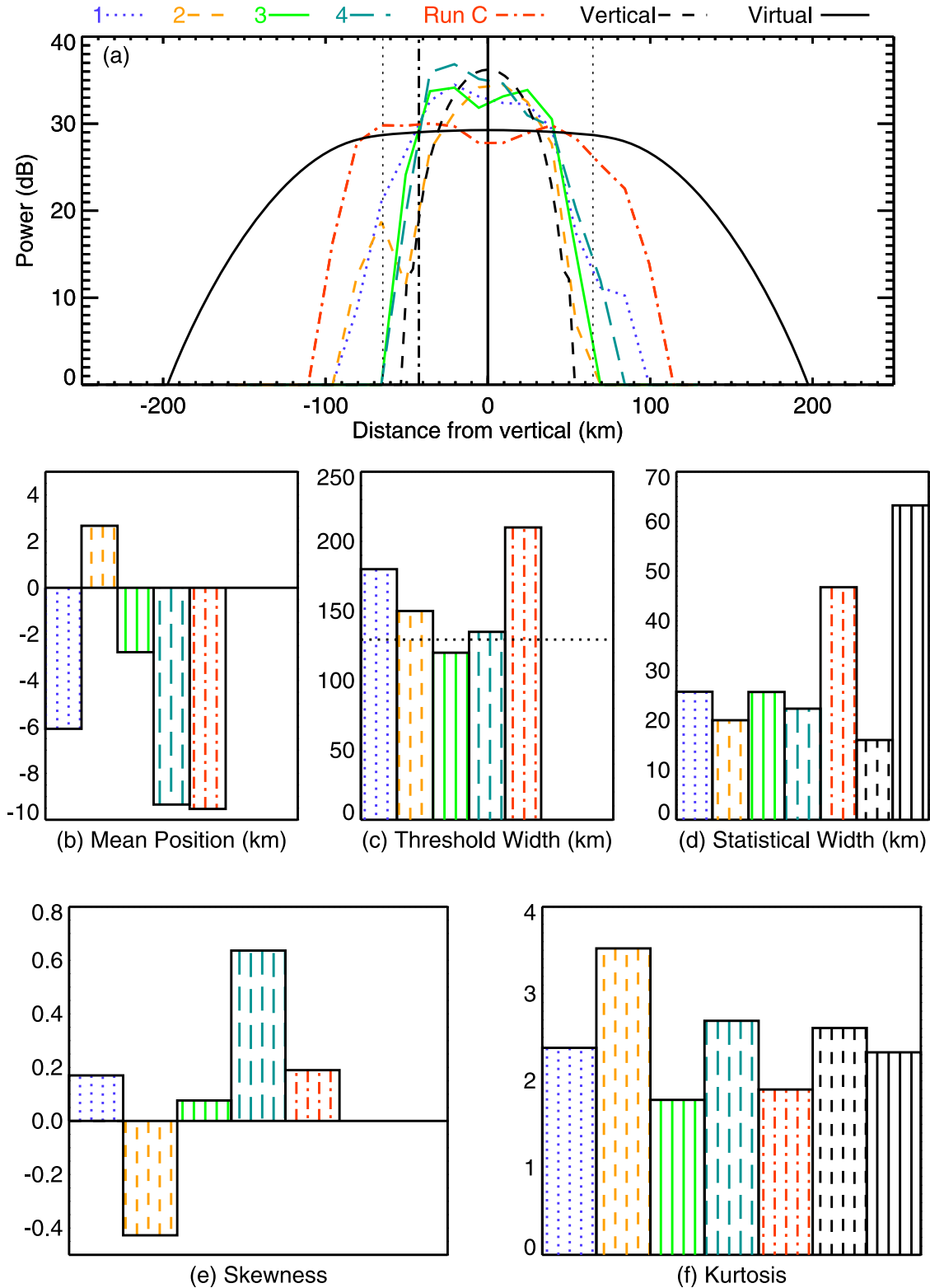


Figure 12. (a) The mean CUTLASS backscatter power distributions measured during beam sweeping run C and four vertical transmissions of the heater beam, the virtual power distribution of Figure 9b, and the vertically transmitted modeled power distribution, in decibels, and (b) mean position, (c) threshold width, (d) statistical width, (e) skewness, and (f) kurtosis of the linear mean backscatter power distributions and the linear virtual and vertical beam power distributions.

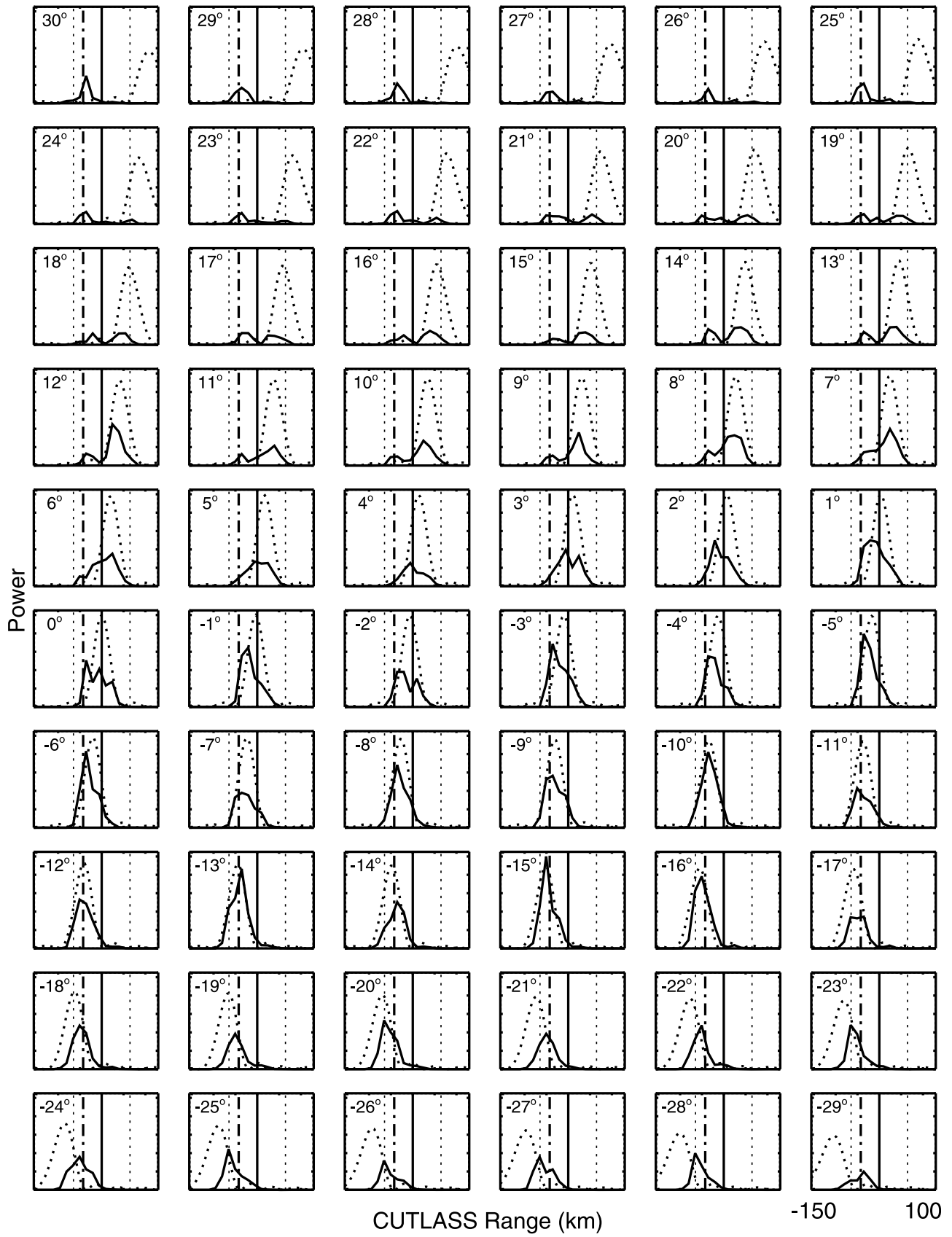


Figure 13

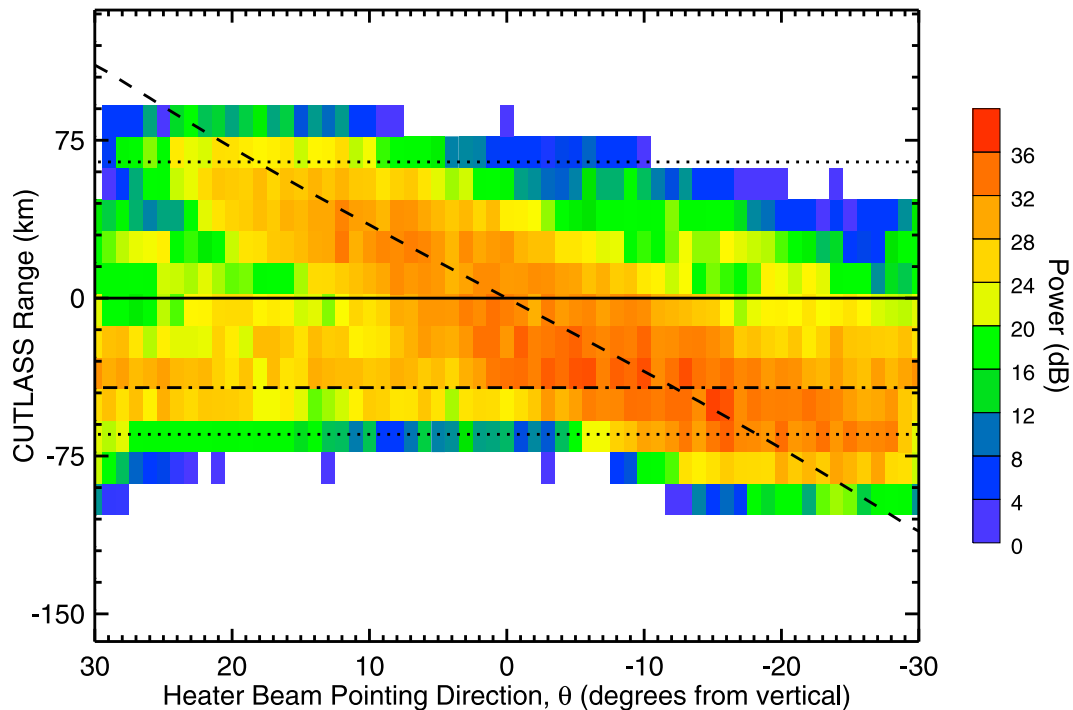


Figure 14. The CUTLASS backscatter power data measured during beam-sweeping run A, averaged over the heater beam pointing direction. The dashed line shows the positions of the peaks of the modeled heater beam power distributions, the solid line indicates the position vertically above the heater along the CUTLASS beam, the dot-dashed line indicates the magnetic field direction, and the dotted lines indicate the upper hybrid width limits.

displayed in Figure 6 (bottom), and the solid horizontal line in Figure 15c indicates the size of the upper hybrid width. The six plots in Figure 15 will now be discussed, with reference to the statistical parameters of the individual beam sweeps presented in Figure 7 when required.

[57] The summed patch power, displayed in Figure 15a, peaks when the heater beam points approximately 10° in the negative direction rather than when the summed power of the modeled heater beam distributions peaks in the vertical heater beam pointing direction. As mentioned in section 6.3.1, Figure 7 demonstrates that during the earlier sweeps of the run the patch power peaked close to where the heater beam pointed vertically, but the peak occurred at more negative beam pointing directions toward the end of the run. This appears to be a result of the amplitude of irregularities measured during each sweep being affected by the decaying irregularities from the preceding sweep. Figure 4 (top) shows a high amplitude at ranges close to -30 km throughout the beam-sweeping run. In the time taken for each sweep to occur, the FAIs do not completely decay at this range, causing the amplitude here to constantly increase. This cumulative effect could explain the observations of a changing position of the maximum summed power such that

a maximum occurs at a negative pointing direction after averaging.

[58] The mean patch position, shown in Figure 15b, steadily changes from slightly positive to negative values as the heater beam pointing direction changes. The mean position of the modeled heater beam power distributions varies between ± 100 km (Figure 6b), while the mean patch position varies between only $+20$ and -50 km. The extent of the patch is therefore considerably less than that of the modeled beam, and this may be due to the width limit at the upper hybrid height. Figure 5 indicates that the main heater beam lies completely outside of the upper hybrid width limits once the angular displacement is greater than 25° . The beam should therefore be unable to generate FAIs at U for the first and last 5 s of each sweep, while the angular displacement lies between 25° and 30° . Figure 14 shows that relatively high-powered irregularities were produced only once a considerable part of the main beam had entered the upper hybrid width region, just before the heater beam pointed at $+20^\circ$. The position of these FAIs is just inside the upper hybrid width region, providing strong evidence of its limiting effect. Irregularities are present at the latter ends of the sweeps, beyond a -20° beam pointing direction, possibly because these are formed closer to the magnetic field

Figure 13. CUTLASS backscatter power data measured during beam-sweeping run A, averaged over the heater beam pointing direction. The sequence of plots represents the change in backscatter power with time as the heater beam direction changes. The solid and dot-dashed lines indicate the vertical and magnetic field directions, respectively, and the dotted lines indicate the upper hybrid width limits. The heater beam pointing direction, θ , is given in the top left of each frame, and the modeled heater beam power distributions are shown using dotted lines.

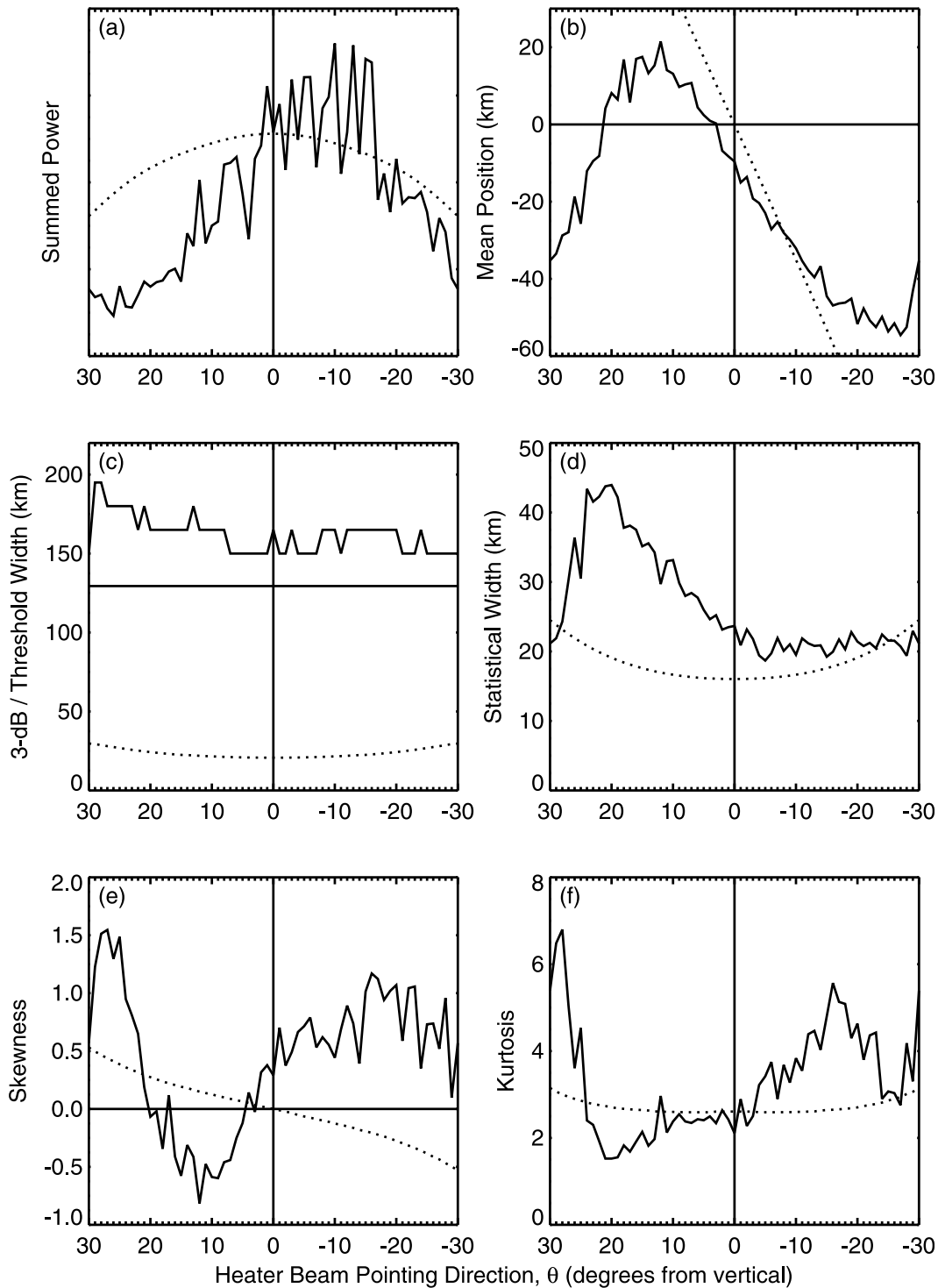


Figure 15. Variation of (a) summed power, (b) mean position, (c) threshold width, (d) statistical width, (e) skewness, and (f) kurtosis with heater beam pointing direction of the averaged backscatter power distributions in Figures 13 and 14 associated with beam-sweeping run A. The horizontal line in Figure 15c indicates the size of the upper hybrid width, and the dotted lines indicate the statistical moments and 3 dB width of the modeled heater beam power distributions at h_U without side lobes.

direction. These irregularities would have a higher power due to heater beam focusing and take longer to decay. However, again, the FAIs do not extend very far beyond the upper hybrid width limit.

[59] The minimum mean patch position has a larger magnitude than the maximum mean patch position, unlike the mean position of the modeled beam, the extent of which is symmetrical about 0. Again, it may be that in the negative

beam pointing directions the heater beam power was focused by the irregularities aligned along the magnetic field direction. The corresponding larger powers would produce the negatively biased mean patch position.

[60] The maximum mean patch position occurs at $\theta = 15^\circ$ rather than at the start of the sweep. Such a large delay was not observed during the first sweep in Figure 12, where the maximum mean position occurred 5 s after the beginning of the sweep, at $\theta = 25^\circ$. The delay, therefore, could be attributed to the time required for the decay of irregularities formed in the negative beam pointing direction. This causes the mean position to be less positive than expected at the start of each sweep except the first.

[61] The threshold width of the FAIs, shown in Figure 15c, decreases from 200 km and then remains approximately constant at around 150 km, close to the 130 km upper hybrid width. The 3 dB width of the modeled heater beam, also plotted in Figure 15c, increases for greater angular displacements from vertical, but, as mentioned, the small 10 km change would not have been resolved by the CUTLASS radar. As the angular displacement of the beam from vertical increases, larger areas of the main beam lie outside of the upper hybrid width limits, as observed in Figure 5. The threshold width of the patch remained predominantly constant during the sweeps. One possible explanation of this is that the side lobes of the beam within the upper hybrid width were sufficiently powerful to sustain the irregularities. It is apparent from Figure 4 that the limits of the upper hybrid width, displayed as dashed lines, signify very well the extent of the patch in both directions. The solid lines in Figure 4 indicate the extent to which the heater rays within the 3 dB width of the main beam were able to reach according to the heater beam model. Since the patch of FAIs did not extend out to this distance, it is apparent that the width of the patch was limited. The threshold width of the patch is considerably larger than the 3 dB width of the modeled heater beam, implying the beam is able to generate FAIs with power from outside of its 3 dB width. The extent of the swept region indicated in Figure 4 is therefore actually greater than that shown.

[62] The statistical width of the patch of FAIs, plotted in Figure 15d, rapidly increases from 20 to 40 km before decreasing to a steady value of approximately 20 km as the heater beam pointing direction approaches vertical. Between transmission angles of $+30^\circ$ and $+25^\circ$ it appears that irregularities remaining from the preceding sweep dominate with a relatively small statistical width, which grows as they decay and become less structured. New irregularities form at more positive ranges once the main beam of the heater enters the upper hybrid width region. The double-peaked power distribution identified in Figures 13 and 14 and caused by the presence of both decaying and newly formed irregularities is responsible for the relatively large statistical width between heater beam transmission angles of $+25^\circ$ and $+10^\circ$. As the beam is pointed closer to the vertical direction, this effect decreases and the statistical width of the patch steadies to 20 km as the backscatter power profile becomes a single-peaked distribution, either via complete decay or through reexcitation of decaying irregularities. As previously mentioned, Figure 13 shows some evidence of reexcitation of decaying irregularities between $\theta = 14^\circ$ and 6° . If reexcitation does occur, the resulting change in patch power

is relatively small since there is no obvious increase at $\theta = 14^\circ$ in Figure 15a. The steady statistical patch width of 20 km matches that of the modeled beam at U without side lobes, as also plotted in Figure 15d.

[63] The decreasing patch skewness observed at the beginning of the sweep in Figure 15e is associated with the decay of FAIs close to -30 km in Figure 14 and the growth of new FAIs close to the 60 km range. Between transmission angles of $+10^\circ$ (northward) and -20° (southward) the patch skewness increases from -1 to $+1$ as the position of the newly formed FAIs gradually shifts from $+15$ km to -75 km, as observed in Figure 14, due to the southward movement of the beam. Between $\theta = -20^\circ$ and -30° the skewness of the patch decreases and approaches zero. In Figure 14 a shift in range of the FAIs due to the motion of the beam is not observed between these transmission angles. This may be due to the self-focusing of the beam power that has been suggested and the consequent slower decay of high power FAIs in this direction, close to the magnetic field. The patch becomes more symmetrical during this time, and the skewness decreases toward zero. The values of patch skewness throughout the sweep are comparable to the skewness of the modeled beam distributions, although the change in patch skewness as the sweep progresses does not match that of the heater beam.

[64] Between transmission angles of $\pm 30^\circ$, the patch kurtosis displayed in Figure 15f first decreases as new FAIs are established alongside decaying ones, producing a relatively wide and flat power distribution, as observed between $\theta = 25^\circ$ and 15° in Figure 13. It then increases as the new irregularities begin to dominate, resulting in the sharpest power profile with the largest value of kurtosis when the heater beam points in the magnetic field direction. Between $\theta = -12^\circ$ and -30° the kurtosis decreases. Apart from the discrepancy close to the magnetic field direction and at the beginning of the sweep when two sets of irregularities are present, the kurtosis of the patch is comparable to that of the modeled beam.

[65] Figure 10 displays excellent agreement between the mean values of skewness and kurtosis of the patch of FAIs created during run C (dotted lines) and of the effective transmitted heater beam power of Figure 9b (green). The skewness of the beam power distribution is zero since there are equal heater transmissions on either side of the vertical pointing direction. The skewness of the patch changes from slightly negative to slightly positive during the course of the beam-sweeping run, and this trend might be due to the observed bias for irregularities to form in the direction of the magnetic field since a distribution with higher power here and lower powers elsewhere within the upper hybrid width limits would have a negative skewness. The negative rather than zero mean patch position is a consequence of the bias of power at negative ranges, as observed in Figure 4. As with the data from run A, which also have a mean patch position more negative than expected, this asymmetry may be due to the self-focusing of the heater beam power, resulting in more powerful striations close to the magnetic field direction. A restriction on the patch extent by the upper hybrid width limits could explain the statistical width of the patch being lower than that of the virtual beam. Figures 11a and 12a demonstrate that the 3 dB points of the virtual beam power distribution are positioned outside of the upper hybrid

width, so a smaller statistical width is expected for the FAIs excited by the beam.

[66] Finally, a dip in the backscatter power profile associated with run C is observed in the vertical direction in Figures 11a and 12a. It is possible that this dip is due to a penetration of the heater beam rays in the region of highest backscatter power. If the electron density in the ionosphere is greatly altered by heating such that the plasma frequency in this region decreases to sufficiently below the heater frequency and irregularity excitation does not occur, then the amplitude of FAIs is likely to be lower than that of the surrounding regions [Fialer, 1974; Minkoff *et al.*, 1974].

8. Summary and Conclusions

[67] Backscatter power profiles measured by the CUTLASS Finland radar during fast and slow heater beam-sweeping experiments at the EISCAT facility have been statistically analyzed. The backscatter data correspond to patches of small-scale, artificial, field-aligned electron density irregularities enhanced by the EISCAT heater. Threshold widths of the CUTLASS backscatter power profiles have been compared to a simple model of the geometrical size of the heated region at the upper hybrid height, and the statistical moments (summed power, mean position, statistical width, skewness, and kurtosis) of the power profiles have been compared to those of modeled heater beam power distributions provided by the EZNEC version 4 software. Data from the EISCAT UHF radar and the EISCAT Tromsø dynamometer have been used to determine the upper hybrid height and peak ionospheric plasma frequency during the heating experiments, respectively.

[68] The dependence of the statistical parameters of the CUTLASS backscatter power profiles on different heater beam pointing directions was investigated. The statistical parameters of CUTLASS backscatter power profiles measured during heater beam sweeping were compared to those measured during static vertical transmissions. Of the three beam-sweeping runs, the patch created during the fastest run most resembled a patch produced by a static vertical heater transmission. Apart from the statistical width, the statistical moments of these were found to agree, indicating the resemblance between a fast heater beam sweep and a static vertical transmission.

[69] The highest backscatter powers were measured in the direction of Earth's magnetic field despite the heater transmitting symmetrically either side of vertical. This bias is attributed to a focusing of the heater beam rays by the electron density depletion along the magnetic field, as also suggested by Rietveld *et al.* [2003] after observing similar effects.

[70] Good agreement between the statistical moments of the patches and the modeled heater beam power distributions without side lobes has been observed. This is the case during the second half of the slowest beam-sweeping run, when the irregularities from the first half of the run have decayed. During the fastest beam-sweeping run, a virtual modeled beam power distribution was used, created from a superposition of individual heater beam power distributions associated with different beam pointing directions. Here again there was an agreement between the statistical moments of the patch power distribution and the modeled

heater beam power distribution. The statistical width of the virtual beam was larger than that of the patch created during the fastest beam sweeps, however, which is thought to be limited by the upper hybrid width.

[71] Statistical results indicate that the heater beam side lobes are able to sustain excited irregularities if not cause enhancement themselves. The largest change in the statistical moments of the heater beam power distributions upon side lobes removal is observed in the kurtoses. It is possible for multiple peaks in the power distribution within a patch of irregularities to combine into a single peak, as observed during the slowest beam-sweeping runs. Therefore, it may be that the statistical moments of the patches match those of either the whole heater beam or the main beam or, more reasonably, values between the two.

[72] As expected, comparisons of the modeled heater beam power distributions with CUTLASS backscatter power distributions indicate that the heater beam has a large influence on the patches of irregularities. However, the analysis of CUTLASS Finland backscatter power profiles during beam-sweeping experiments has provided strong evidence in favor of the upper hybrid theory of irregularity generation. The theory was tested by considering the effects of moving the heater beam outside of the upper hybrid width limits. No irregularity excitation was observed outside of the upper hybrid width limits.

[73] Many patches of irregularities excited by the EISCAT heater display a bias of power in the direction of Earth's magnetic field. This may be due to focusing of the heater beam, the time scale for which is a few tens of seconds. Backscatter power profiles corresponding to relatively slow beam-sweeping experiments were observed to display a larger bias of power in the direction of the magnetic field, indicating the effect of an instability requiring some tens of seconds to become established. Therefore, it is likely that the observed bias of power in the magnetic field direction within patches of irregularities is due to self-focusing of the heater beam power by the field-aligned irregularities.

[74] Ideally it would be possible to make comparisons with a number of additional beam-sweeping experiments; however, there are no data available for this. It is hoped that experiments carried out at the EISCAT heater in the future may include some that are influenced by the results and discussion presented in this paper.

[75] **Acknowledgments.** Many thanks are due to the EISCAT Scientific Association for operating and maintaining the Tromsø heater. CUTLASS is supported by the UK Science and Technology Facilities Council, the Finnish Meteorological Institute, and the Swedish Institute of Space Physics. The authors would also like to thank D. M. Wright, J. A. Davies, and the technical staff for valuable support during the experimental campaigns.

[76] Amitava Bhattacharjee thanks Christian Haniuise and Brett Isham for their assistance in evaluating this paper.

References

- Bernhardt, P. A., and L. M. Duncan (1982), The feedback-diffraction theory of ionospheric heating, *J. Atmos. Terr. Phys.*, *44*, 1061–1074, doi:10.1016/0021-9169(82)90018-6.
- Bond, G. E. (1997), The interaction of radio waves with the auroral ionosphere, Ph.D. thesis, Univ. of Leicester, Leicester, U. K.
- Bond, G. E., T. R. Robinson, P. Eglitis, D. M. Wright, A. J. Stocker, M. T. Rietveld, and T. B. Jones (1997), Spatial observations by the CUTLASS

- coherent scatter radar of ionospheric modification by high power radio waves, *Ann. Geophys.*, *15*, 1412–1421, doi:10.1007/s00585-997-1412-4.
- Cohen, R., and J. D. Whitehead (1970), Radio reflectivity detection of artificial modification of the ionospheric F layer, *J. Geophys. Res.*, *75*, 6439–6445, doi:10.1029/JA075i031p06439.
- Das, A. C., and J. A. Fejer (1979), Resonance instability of small-scale field-aligned irregularities, *J. Geophys. Res.*, *84*, 6701–6704, doi:10.1029/JA084iA11p06701.
- Davies, K. (1966), *Ionospheric Radio Propagation*, Dover, New York.
- Dhillon, R. S. (2001), Radar studies of natural and artificial waves and instabilities in the auroral ionosphere, Ph.D. thesis, Univ. of Leicester, Leicester, U. K.
- Evans, J. V. (1969), Theory and practice of ionosphere study by Thomson scatter radar, *Proc. IEEE*, *57*, 496–530, doi:10.1109/PROC.1969.7005.
- Fialer, P. A. (1974), Field-aligned scattering from a heated region of the ionosphere: Observations at HF and VHF, *Radio Sci.*, *9*, 923–940, doi:10.1029/RS009i011p0923.
- Greenwald, R. A., et al. (1995), DARN/SUPERDARN: A global view of the dynamics of high latitude convection, *Space Sci. Rev.*, *71*, 761–796, doi:10.1007/BF00751350.
- Honary, F., A. J. Stocker, T. R. Robinson, T. B. Jones, N. M. Wade, P. Stubbe, and H. Kopka (1993), EISCAT observations of electron temperature oscillations due to the action of high power HF radio waves, *J. Atmos. Terr. Phys.*, *55*, 1433–1435, doi:10.1016/0021-9169(93)90109-C.
- Hughes, J. M., W. A. Bristow, R. T. Parris, and E. Lundell (2003), SuperDARN observations of ionospheric heater-induced upper hybrid waves, *Geophys. Res. Lett.*, *30*(24), 2276, doi:10.1029/2003GL018772.
- Jones, T. B., T. R. Robinson, P. Stubbe, and H. Kopka (1982), Phase changes induced in a diagnostic radio wave passing through a heated region of the auroral ionosphere, *J. Geophys. Res.*, *87*, 1557–1564, doi:10.1029/JA087iA03p01557.
- Jones, G. O. L., C. J. Davis, and R. E. Stockwell (2000), Dynasonde observations of electron concentration gradients above Tromsø, *J. Atmos. Sol. Terr. Phys.*, *62*, 1385–1391, doi:10.1016/S1364-6826(00)00156-5.
- Jones, T. B., T. R. Robinson, P. Stubbe, and H. Kopka (1986), EISCAT observations of the heated ionosphere, *J. Atmos. Terr. Phys.*, *48*, 1027–1035, doi:10.1016/0021-9169(86)90074-7.
- Milan, S. E., T. K. Yeoman, M. Lester, E. C. Thomas, and T. B. Jones (1997), Initial backscatter occurrence statistics from the CUTLASS HF radars, *Ann. Geophys.*, *15*, 703–718, doi:10.1007/s00585-997-0703-0.
- Minkoff, J., P. Kugelman, and I. Weissman (1974), Radio frequency scattering from a heated ionospheric volume: I. VHF/UHF field-aligned and plasma-line backscatter measurements, *Radio Sci.*, *9*, 941–955, doi:10.1029/RS009i011p0941.
- Mjølhus, E., and T. Flå (1984), Direct access to plasma resonance in ionospheric radio experiments, *J. Geophys. Res.*, *89*, 3921–3928, doi:10.1029/JA089iA06p03921.
- Mjølhus, E., E. Helmersen, and D. F. DuBois (2003), Geometric aspects of HF driven Langmuir turbulence in the ionosphere, *Nonlinear Process. Geophys.*, *10*, 151–177.
- Noble, S. T., and F. T. Djuth (1990), Simultaneous measurements of HF-enhanced plasma waves and artificial field-aligned irregularities at Arecibo, *J. Geophys. Res.*, *95*, 15,195–15,207, doi:10.1029/JA095iA09p15195.
- Rietveld, M. T., H. Kohl, H. Kopka, and P. Stubbe (1993), Introduction to ionospheric heating at Tromsø: I. Experimental overview, *J. Atmos. Terr. Phys.*, *55*, 577–599, doi:10.1016/0021-9169(93)90007-L.
- Rietveld, M., B. Isham, H. Kohl, C. La Hoz, and T. Hagfors (2000), Measurements of HF-enhanced plasma and ion lines at EISCAT with high-altitude resolution, *J. Geophys. Res.*, *105*, 7429–7439, doi:10.1029/1999JA900476.
- Rietveld, M. T., M. J. Kosch, N. F. Blagoveshchenskaya, V. A. Kornienko, T. B. Leysner, and T. K. Yeoman (2003), Ionospheric electron heating, optical emissions, and striations induced by powerful HF radio waves at high latitudes: Aspect angle dependence, *J. Geophys. Res.*, *108*(A4), 1141, doi:10.1029/2002JA009543.
- Rishbeth, H., and A. P. van Eyken (1993), EISCAT: Early history and the first ten years of operation, *J. Atmos. Terr. Phys.*, *55*, 525–542, doi:10.1016/0021-9169(93)90002-G.
- Rishbeth, H., and P. J. S. Williams (1985), The EISCAT ionospheric radar: The system and its early results, *Q. J. R. Astron. Soc.*, *26*, 478–512.
- Robinson, T. R. (1989), The heating of the high latitude ionosphere by high power radio waves, *Phys. Rep.*, *179*, 79–209, doi:10.1016/0370-1573(89)90005-7.
- Robinson, T. R. (2002), Effect of multiple scatter on the propagation and absorption of electromagnetic waves in a field-aligned-striated magnetoplasma: Implications for ionospheric modification experiments, *Ann. Geophys.*, *20*, 41–55.
- Robinson, T. R., A. J. Stocker, G. Bond, P. Eglitis, D. Wright, and T. B. Jones (1997), O and X mode heating effects observed simultaneously with the CUTLASS and EISCAT radars and low power HF diagnostics at Tromsø, *Ann. Geophys.*, *15*, 134–136.
- Robinson, T. R., A. Stocker, G. Bond, P. Eglitis, D. Wright, T. B. Jones, and M. T. Rietveld (1998), First CUTLASS-EISCAT heating results, *Adv. Space Res.*, *21*, 663–666, doi:10.1016/S0273-1177(97)01000-4.
- Schlegel, K. (1996), Coherent backscatter from ionospheric E region plasma irregularities, *J. Atmos. Terr. Phys.*, *58*, 933–941, doi:10.1016/0021-9169(95)00124-7.
- Sedgemore, K. J. F., P. S. J. Williams, G. O. L. Jones, and J. W. Wright (1996), A comparison of EISCAT and Dynasonde measurements of the auroral ionosphere, *Ann. Geophys.*, *14*, 1403–1412, doi:10.1007/s005850050401.
- Spiegel, M. R. (1972), *Theory and Problems of Statistics*, McGraw-Hill, Singapore.
- Stocker, A. J., F. Honary, T. R. Robinson, T. B. Jones, P. Stubbe, and H. Kopka (1992), EISCAT observations of large scale electron temperature and electron density perturbations caused by high power HF radio waves, *J. Atmos. Terr. Phys.*, *54*, 1555–1572, doi:10.1016/0021-9169(92)90163-F.
- Stubbe, P., et al. (1982a), Ionospheric modification experiments in northern Scandinavia, *J. Atmos. Terr. Phys.*, *44*, 1025–1041, doi:10.1016/0021-9169(82)90015-0.
- Stubbe, P., H. Kopka, T. B. Jones, and T. Robinson (1982b), Wide band attenuation of radio waves caused by powerful HF waves: Saturation and dependence on ionospheric variability, *J. Geophys. Res.*, *87*, 1551–1555, doi:10.1029/JA087iA03p01551.
- Thome, G. D., and D. W. Blood (1974), First observations of RF backscatter from field-aligned irregularities produced by ionospheric heating, *Radio Sci.*, *9*, 917–921, doi:10.1029/RS009i011p0917.
- Yampolski, Y. M., V. S. Beley, S. B. Kascheev, A. V. Koloskov, V. G. Somov, D. L. Hysell, B. Isham, and M. C. Kelley (1997), Bistatic HF radar diagnostics induced field-aligned irregularities, *J. Geophys. Res.*, *102*, 7461–7467, doi:10.1029/97JA00037.

R. S. Dhillon, M. Lester, S. E. Milan, T. R. Robinson, H. Shergill, and T. K. Yeoman, Department of Physics and Astronomy, University of Leicester, University Road, Leicester, LE1 7RH, UK. (hs38@ion.le.ac.uk)